REPORT DOCUMENTATION PAGE

Form Approved
OMB No. 074-0188

1. AGENCY USE ONLY (Leave blank)	2. REPORT DATE **February 11, 2010**	3. REPORT TYPE AND DATES COVERED Final Report; 6/15/06 – 12/14/09

4. TITLE AND SUBTITLE
Stimulated Electron Desorption Studies from Microwave Vacuum Electronics / High Power Microwave Materials

5. FUNDING NUMBERS
FA9550-06-1-0451

6. AUTHOR(S)
Robert A. Schill, Jr. (PI)

7. PERFORMING ORGANIZATION NAME(S) AND ADDRESS(ES)

University of Nevada Las Vegas
Electrical and Computer Engineering
4505 Maryland Parkway
Las Vegas, Nevada 89154-4026

8. PERFORMING ORGANIZATION REPORT NUMBER
DNA

9. SPONSORING / MONITORING AGENCY NAME(S) AND ADDRESS(ES)

AFOSR/NE
875 N. Randolph St, Rm 3-112
Arlington, VA 22203

10. SPONSORING / MONITORING AGENCY REPORT NUMBER

11. SUPPLEMENTARY NOTES

12a. DISTRIBUTION / AVAILABILITY STATEMENT

12b. DISTRIBUTION CODE
DIST CODE A:
UNLIMITED

13. ABSTRACT *(Maximum 200 Words)*
This DEPSCoR research examined secondary electron emission (SEE) from thin films and from a warm metal material. Evidence suggests that backscattered electrons as a whole have a preferred scattering direction with a distribution that is dependent on the type of surface treatment. Secondary electron emission was studied from a chemical polished niobium sample during transient cooling from ~360 $^{\circ}$K to ~ 293 $^{\circ}$K. It was observed that: 1) "True" secondary electron distributions tend to exhibit a shifted Gaussian-like spatial distribution; 2) a metal structure undergoing transient cooling exhibits some small overall average tendencies on the scattering process; 3) the change in the mean number of scattered electrons seems to increase on average as the metal sample cools; and 4) the emitted backscattered electron cluster appears to be scattered normal to the sample surface for the temperature range considered. A strong AFRL/UNLV collaboration examined four different types of samples. Based on single, pulsed, emission tests, improvements in minimizing secondary electron emission count were observed with the coated copper substrates. Within experimental bounds, secondary electron emission hardening may not take place in all films. Further, the count and distribution are dependent on the primary electron beam's target angle.

14. SUBJECT TERMS	15. NUMBER OF PAGES 47
	16. PRICE CODE

17. SECURITY CLASSIFICATION OF REPORT	18. SECURITY CLASSIFICATION OF THIS PAGE	19. SECURITY CLASSIFICATION OF ABSTRACT	20. LIMITATION OF ABSTRACT

Final Report 6/15/06 – 12/14/09
FA9550-06-1-0451
Stimulated Electron Desorption Studies from Microwave Vacuum Electronics / High Power Microwave Materials

By

Robert A. Schill, Jr.
Director and Founder of the Energy Materials Interaction Technology
Initiative of Nevada (EMITION) Center
Department of Electrical and Computer Engineering
University of Nevada Las Vegas
Las Vegas, Nevada 89154-4026

Abstract

Secondary electron emission (SEE) can potentially lead to beam instabilities, material degradation, beam closure (shorting or pulse shortening), and R.F. breakdown. Under certain conditions, SEE may be desired as a source of electrons for a high power microwave device. Material surface physics, morphology, and possibly the state of the material play a role in the emission process. This DEPSCoR research effort examined secondary electron emission from thin films of potential interest for anode application in high power microwave devices and SEE from a warm metal material. The study ultimately led to a strong AFRL collaboration (Materials and Manufacturing Directorate at Wright-Patterson Air Force Research Laboratory). Absolute and comparative studies were performed with a number of results. Strong evidence suggests that backscattered electrons as a whole have a preferred scattering direction with a distribution that is dependent on the type of surface treatment. Therefore, it may be possible to segregate backscattered electrons from true secondary electrons allowing for optimal anode designs in managing energetic and non energetic electrons. Secondary electron emission was studied from an aged, buffered chemical polished niobium sample during transient cooling from a measurable ~360 $^\circ$K temperature to near room temperature. It was observed that: 1) The "True" secondary electron distribution (as we define it) tends to exhibit a shifted Gaussian-like spatial distribution for the surface grade under test; 2) There are indications that a metal structure undergoing transient cooling exhibits some small overall average tendencies on the scattering process; 3) Although not conclusive, the change in the mean number of scattered electrons seems to increase on average as the metal sample cools; and 4) The emitted backscattered electron cluster appears to be scattered normal to the sample surface within the temperature range considered (~360 $^\circ$K to 293 $^\circ$K). This appears to agree with past cold study findings (>50 $^\circ$K). The AFRL/UNLV collaboration examined three potential anode coatings (TiN, AlTiN, TiCN) on a polished, oxygen free copper substrate, one titanium-on-copper laminate, and a coating free, UNLV polished, copper wedge with noticeable grain imperfections. Based on single, pulsed, emission tests noticeable improvements in secondary electron emission count were observed with the coated copper substrates. Although not conclusive, there is evidence that secondary electron emission hardening based on a single location studies illuminated with up to fifty short duration, low energy, low current electrons does not take place in all films. It is observed that the secondary electron emission count and distribution are dependent on the beam's angle relative to the surface of the film. Currently, morphology and molecular studies of the different films are being conducted at AFRL to this end.

I. Introduction

The Department of the Defense's (DOD) past, present, and future invested interests in high power microwave (HPM) originates from application needs in areas as directed energy weapons, global awareness of strategic and tactical situations, space communication, and environment interrogation radar systems. Here, high power microwaves (HPM) denote sources producing coherent electromagnetic radiation from 1 GHz to 100 GHz with an instantaneous peak power of at least 100 MW and more towards GW peaks.[1,2] Future HPM devices required to achieve these needs must approach one or more of the following goals: 1 kA/cm^2 current densities, few kHz repetition pulse rates, subnanosecond pulse bursts, and a kilo-Joule per pulse energies. In achieving these goals, high power microwave devices may potentially suffer from beam instabilities, multipacting, pulse shortening, material degradation, and rf breakdown if not properly designed. Material studies play a significant role in mitigating these effects while pursuing DOD HPM goals. Gas desorption, secondary electron emission, high material vapor pressures, poor material quality, low vacuum pressure environments, electron induced outgassing, and uncontrolled field emission undesirably enable breakdown. The DOD moves toward cleaner vacuum electronics practices to enhance current source technologies. For example, past vacuum tube environments range between 10^{-5} to 10^{-7} Torr. DOD's direction towards ultra-high vacuum environments on the order of 10^{-9} Torr and lower allow for source longevity. In conjunction, future baking and strict surface conditioning protocols offers better source performance as evidenced by the success stories in the vacuum industry. As the state-of-the-art advances, even these practices find their limits. *The conditioning properties of the source walls, bulk material type, and bulk material quality, entwined with economical considerations, play a significant role in dictating both secondary electron emission and stimulated electron desorption yields effecting source operation.*

Secondary electron emission (SEE) can potentially lead to beam instabilities, material degradation, beam closure (shorting or pulse shortening), and R.F. breakdown. Just as important, secondary electron emission may be used as a mechanism for electron production of interest to some high power microwave sources (e.g., spent electrons returned to the magnetron cathode may be used as a primary beam to generate secondary electrons on the cathode as a source for microwave production purposes). When electrically charged particles with sufficient kinetic energy impinge on a solid surface, this surface may emit electrons. The emitted electrons are called secondary electrons and the incident electrons are called primary particles. Secondary electrons can be differentiated into three groups, namely:[3,4] I. elastically reflected primary electrons, II. inelastically backscattered primary electrons, and III. true secondary electrons. When the electrons penetrate the metal surface, the free electrons inside the metal respond to the non-equilibrium Coulombic forces being generated thereby resulting in electron transport within or possibly from the supporting medium. External energy is required in order for the electrons to eject from the metal surface. The minimum amount of energy require for the electron to be emitted is known as the work function. The secondary electron emission coefficient δ of a material is defined as the ratio of the secondary electron current emitted from the surface of the sample under test to the primary electron current incident on the sample. The secondary electron emission yield is an important parameter of the material; the yield depends on many factors such as the primary beam energy and angle of incidence, the coating and the condition of the surface under test, and the bulk material of the sample. Conservation of charge is important in establishing the secondary electron yield and the spatial distribution of secondary electrons. Past SEE studies have deduced secondary electron yield by invoking a conservation of charge without the need to experimentally account for all measurable or by assuming that each experiment is repeated in the same fashion. Typically, the latter is used when examining the spatial distribution of the secondary electrons. This assumption is weak since the so called cumulative dose of electrons can change the surface properties of the material under test. The technique posed in this paper minimizes the need to impose an energy conservation relation and allows one to study the spatial distribution of secondary electrons without the need to repeat the experiment each time the sensor is spatially relocated. Material surface physics and possibly the state of the material play a role in the emission process. Particular

attention to bulk material type and surface morphology, coatings, and surface impurities will be required in the design of high power microwave devices. Although high power microwave tubes employ high current and high energy beams, *it is hypothesized that valuable surface physics interactions are masked by other dominant mechanisms (e.g., temperature) that arise in the overall beam-target interaction process. This makes it difficult to study the underlying physics of secondary electron emission (SEE) which in turn lessens the chance to understand and thoughtfully modify or use the effect. Consequently, low level primary electron beam currents (typically 0.5 pA or less) are used to probe the surface characteristics of coated metals examining the SEE fingerprint unique to the material. The secondary electrons generated from the low level currents are detected with a particle position detector sensitive enough to detect, count, and spatially locate individual electrons. Because the secondary electron yield is higher at low primary electron energies, experiments were performed with low beam energies ($\leq 1 keV$).* Grant number FA9550-06-1-0451 provides DEPSCoR funding, in conjunction with a DURIP equipment grant and initial seed funding, to investigate the spatial distribution (and the evolution of the distribution) of secondary electron emission stimulated by low current, 1 keV and lower energy primary electron beams impinging on metallic target materials with AFRL coatings for potential use in high power microwave devices. Furthermore, an important secondary emphasis has been directed towards establishing an experimental test stand that measurably accounts for nearly all of the charge originating from the gun to scattering from the target material to the detector and wall regions. The following questions underpinning this basic research effort are:

1. *How do primary sources of pulsed electrons alter the surface and/or bulk properties of a material under test over time and affect energy deposition mechanisms of the medium? Can one implement these properties to condition or recondition the surface of the sample minimizing undesired emission processes?*
2. *What influence do contaminants, coatings and composites, and thermal gradients have on SEE?*

This final report will address the studies undertaken over the past three plus years.

Numerous students and laboratory staff members were supported under this grant. Minimal stipends were provided to two staff members (Mr. Stan Goldfarb and Dr. Richard Kant) that volunteer their time in both the experimental and theoretical studies of secondary electron emission. Volunteers, rich in knowledge, pass their life-long experiences on to students and staff. They are an important addition to the group since many of their experiences and explanations may not be found in books or literature. The grant supports a number of undergraduate students. ROTC undergraduate Nathan Lehman graduated in the spring of 2008 and has been working at Edwards Air Force Base in California. Recently, he has decided to pursue a graduate degree with ambitions to become an Electromagnetics instructor to future Air Force personnel. Nathan has already passed on his UNLV laboratory experiences to Air Force personnel in regards to pulsed power devices. Undergraduate Sean Andersen will be joining my research group at UNLV as a graduate student (Masters program) in the fall of 2010. During the duration of the grant, one graduate student completed her Masters degree. She joined the EMITION Center staff in 2008. Her job in part is to maintain and operate the SEE test stand. Due to the nature of the research, all students gain some form of hands-on vacuum science/technology and mechanical machining outside of their electrical engineering disciplines. Further, depending on the stage of the research, they are exposed to electromagnetic noise issues and mitigation techniques that arise when working with extremely low currents; they obtain hands-on experience with microwave sources and devices; they obtain some degree of material science experience; and etc. Hands-on electromagnetic experiences are tied to their course studies. Table 1 summarizes funded personnel associate with the research endeavor.

Table 1: Funded personnel associated with the research effort during the period 9/2006 to 12/2009.

Personnel (Citizenship)	Position / Period	Effort
Shaoru Garner (US)	**Grad** (MS) / 9-05 to 12-07	Thesis directed - Examining the charge accountability in the SEE Test Stand and establishing Test Stand enhancements. (MS Thesis: Completed 11/07)
Sheldon Johnson (US)	**Undergrad**. / 7-06 to 12-06	Helps maintain test stand both electrically and mechanically. Works on MAGIC simulation.
Tak Chang (Stud. Visa)	**Undergrad.** / 7-06 to 5-07	Some simulation with MAGIC and hands on laboratory helper
Nathan Lehman (US)	**Undergrad.** / 5-07 to 5-08	Electrical and vacuum engineer
Rafael Ybarra (US)	**Undergrad.** / 5-07 to 9-07	Machinist and electrical engineer
Dr. Richard Kant (US)	**Volunteer** / 7-05 to 6-07	Aided in experimental studies. He also intimately developed AVAL2 an enhanced SEE Monte Carlo code.
Dr. Ved Nayyar (US permanent residency '09)	**Staff-Volunteer** / 1-07 to 4-08	Proposal writing leading to new applications and research for the SEE test stand
Shaoru Garner (US)	**Staff** / 1-08 to 12-09	Engineering Research Associate – Operates and modifies the SEE test stand. Trains students on the test stand. Responsible for involved MAGIC simulations and analysis interpretation associated with SEE test stand. Aids in documentation and paper writing.
Kris Buchanan (US)	**Undergrad.** / 12/08 to 7/09	Electrical and vacuum engineer.
Sean Andersen (US)	**Undergrad.** / 10/08 to 12-09	Modeler and electrical and vacuum engineer. MATLAB codes developed with application to various data analyses.
Gopi Krishna (Stud. Visa)	**Graduate** (MS) / 9/08 to 5/09	*Supported with a teaching assistantship*. Worked on the Monte Carlo SEE code. Developed flow chart of existing code.
Jackie Schill (US)	**Undergrad. /** 4/08 – 8/09	In part developed the three dimensional artwork for conferences, presentations, and reports.
Mr. Stan Goldfarb (US)	**Volunteer** / 7-05 to 12-09	Vacuum specialist – Helps train students in vacuum theory and technology. Works with vacuum systems and modifications to such systems.

The efforts of this research period resulted in conference papers and/or poster slides that were disseminated to Dr. Joan Yater from the Naval Research Laboratory (NRL) and Dr. Edl Schamlioglu's group at the University of New Mexico (UNM). Dr. Joan Yater has been working on high beam current, high beam energy secondary electron emission from high power microwave (HPM) materials under test with a variable position Faraday cup detector. Dr. Schamlioglu's group studied the dose properties of HPM materials when illuminated with various electron beam energies and current. The interactions resulted in the dissemination of results and/or discussion of technical issues. Some initial results were also disseminated to Dr. Don Shiffler at Kirkland AFRL. The latter has led to a formal oral presentation with scientists and engineers in the Materials and Manufacturing Directorate, Wright Patterson AFRL in Dayton Ohio (Dr. Steven Fairchild [AFRL], Dr. John Boeckl [AFRL], Dr. Timothy Peterson [AFRL], Dr. Kent Averett [AFRL], and Dr. Howard Smith [Triboligix Inc.]).on 7-28-08. The presentation resulted in a strong collaborative research effort formed with the Wright-Patterson AFRL folks regarding the mitigation and/or handling of SEE effects from anodes. A number of studies conducted over the year-and-a-half plus have lead to interesting discoveries some of which will be discussed in this final report. We are currently developing a paper regarding the collaboration effort.

Over the grant duration, Drs. Larry Ludeking and Andrew Wood from ATK Mission Research worked closely with the UNLV group in learning and implementing the MAGIC code to characterize UNLV's SEE Test Stand and to study secondary electron emission from materials under test in the test stand. A number of modifications in the MAGIC code were guided by the constraints of the UNLV SEE Test Stand. The unique novel nature of the UNLV Test Stand has required the assistance and cooperation of a number of vendors working jointly with UNLV to extend the envelope of their product for our specific applications. It is to be understood that the test stand existed prior to AFOSR grants and had to be modified for absolute measurements. In many cases, ours and other vendors' constraints fell outside of typical product specifications resulting in long discussions (typically months to over a year) leading to workable compromises and interpretations. These vendors are identified below.

Names (Company)	Efforts
Drs. Jagutzki and Czasch (RoentDek GmbH)	Their particle position detector was not designed to work in the current environment of the SEE Test Stand. Specific knowledge of their product was crucial in interpreting measured results and limitations of the product. A number of micro issues including direct and stray current management, device longevity and robustness, particle losses, required changes in high voltage biasing, MCP constraints (voltage, losses, and saturation) and degradation, electron management of data, and time stamped computer data management issues required specific attention in order to realize absolute measurements.
Drs. Staib and Polivka (Staib Instruments Inc.)	Aided in modifying an electron beam drift tube to be compatible with their electron gun. Detector constraints required operating their electron gun outside of the gun's specifications. Staib Instruments worked closely with UNLV in learning how to stabilize their instrument with repeatability in beam current. It is very difficult to extend an existing gun to operate outside of specifications in low beam current mode at low energies with a large working distance. Funding was not available to purchase a new gun.
Mr. Mike Ackeret (Transfer Engineering Inc.)	Transfer Engineering's expertise in specialty UHV work and machining propelled the research effort forward at a pace that allowed us to meet most of our deadlines. In some cases, they integrated other's products into the modifications they helped design for the test stand. With UNLV guidance, Transfer Engineering designed and built the original UNLV SEE Test Stand.

Grant highlights and activities are bulleted below:

- A DURIP equipment proposal leading to an equipment grant was written and secured. This allowed for controlled sample temperature studies to be conducted. Results were presented at ICOPS 2009.
- A Masters thesis was completed; Title: Conservation of Charge in SEE Test Stand.
- Working with ATK Mission Research, a MAGIC routine was modified to study SEE from a single charge statistically modeled as a large charge ensemble composed of many fractions of a charge. The simulation aided in verifying primary beam current thresholds allowed for *absolute* secondary electron emission measurements.
- Developed experimental techniques to study *absolute* SEE measurements in the test stand pushing the limits of the gun and detector beyond manufacturer specifications. Sensor development and implementation provided physical meaning to measurements made by the particle position detector.
- Incorporated sample, grid, and tube diagnostics and isolation schemes. Shielding and stray current management issues resolved.

- Explored a non-intrusive, non-destructive technique to measure low beam currents. Sensor development led to a UNLV patent disclosure (UNLV patent application is in process 8/21/08).
- Some initial *absolute* studies of SEE were performed on UNLV polished copper. With the aid of previous SEE research experience, results tend to strongly suggest that backscattered electrons may be differentiated from true secondary electrons. This result finds application in anode design. High energy backscattered electrons may be separated from true low energy secondary electrons. Consequently, electron-capturing schemes for high energy electrons may be segregated from electron-capturing schemes for low energy electrons. This may be of significance if films used to capture electrons are prone to damage if exposed to electrons within a certain range of energy levels conducive with the backscattered electrons.
- Results were disseminated at the 2009 ICOPS, 2008 IEEE Power Modulator, and 2007 PPPS conferences.
  - Shaoru Garner, Robert A. Schill, Jr., Sean Andersen, Kris Buchanan, and Jackie Schill, *Electron Stimulated Secondary Electron Emission from a Warm Metal Surface,* **IEEE ICOPS 2009**, San Diego, California, May 31 - June 5, 2009 (*Poster Session), abstract.*
  - Shaoru Garner, Nathan Lehman, and Robert A. Schill, Jr., *Spatial Distribution of Electron Stimulated Electron Desorption from a Metal Surface*, **2008 IEEE International Power Modulator and High Voltage Conf.**, (ed. Hulya Kirkici), Las Vegas, NV, May 27-31, 2008, p. 303-306.
  - Shaoru Garner, Robert A. Schill, Jr., and Richard Kant, *Conservation of Charge in the Secondary Electron Emission Test Stand at UNLV*, **IEEE PPPS 2007**, Albuquerque, New Mexico, June 17-22, 2007 (*Poster Session), abstract.*
- Promoted interest in the Air Force Research Laboratory community to make use of the novel test stand for SEE studies from materials used in high power microwave devices. Built a strong collaboration with Materials and Manufacturing Directorate, Wright Patterson AFRL in Dayton Ohio.
- Flow charted an existing C++ SEE Monte Carlo code (code developed at UNLV with seed funding) for future discussions with code developers (Simplified and detailed versions)
- Conducted SEE experiments on Cu as it was cooling
  - Influenced by the distribution of BSE based on how we define "True" SE, the "True" SE distribution tends to exhibit a shifted Gaussian like distribution for the 30° grade.
  - There are indications that metal structures undergoing transient cooling over a small range of temperatures (360° to 293° K) exhibits some small overall average tendencies on the scattering process.
  - The change in the mean number of scattered electrons seems to increase on average as the metal sample cools. This is not conclusive in all experimental data sets.
  - Backscattered electron bunch appears to be scattered normal to the sample surface
- Conducted numerous SEE studies on thin films coating oxygen free copper slabs at room temperature for electron beams obliquely incident on the target (0°, 10°, and 30° grades)

This report is divided into the following sections. Section II provides a calibration and test study of the SEE Test Stand. A brief discussion of modeling studies is presented in Section III. Highlights of SEE from a warm metal sample in transient cooling phase are found in Section IV. Section V, provides an in-depth discussion on the research collaboration with AFRL with results and tendencies explained within the limits of the experiment. The report closes in Section VI with a summary of the research as it pertains to the two questions that motivated the research endeavor.

II. SEE Test Stand – Calibration and Test Study

The final report for AFOSR grant number FA9550-05-1-0284 and thesis Shaoru Garner, <u>Conservation of Charge In Secondary Electron Emission Test Stand</u>, UNLV, December 2007 provides an in-depth discussion on the accountability of the currents and charges in the UNLV SEE Test Stand. This topic will not be presented here. Some of the calculations and deductions found in these sources are employed in this report.

It was hypothesized that low current primary beams are needed to study the beam-target surface physics leading to secondary electron emission (SEE). Being able to study the spatial distribution of the emitted secondary electrons requires the ability to detect and record the spatial coordinates of individual electrons captured by the detector. Figure 1 depicts a typical experimental setup consisting of a Staib electron gun, an isolated beam drift tube, a hexanode delay line with a chevron microchannel plate (MCP) stack, an isolated grid, an isolated target (copper in this case), and a grounded holder. A manipulator arm is used in positioning the target under vacuum when needed. Figure 2 displays the external components of the SEE Test Stand. Both calculated and experimentally determined primary beam currents of less than a pico-ampere are required so to avoid saturating and damaging the particle position detector. Such small currents are difficult to work with and to detect in an electromagnetic noise environment. Great care was taken to ground and shield the test stand to minimize external noise from influencing the experimental measurements. Internal to the machine, special grounding techniques were used to minimize microphonic effects resulting from pump vibration. During some of the experimental runs (very few), all sources of mechanical vibration (including cryopumps) had to be switched off intermittently at the time data was taken.

Electron Gun

Isolated Beam Drift Tube

Hexanode Delay Line and Anode

MCP Stack

Isolated Grid

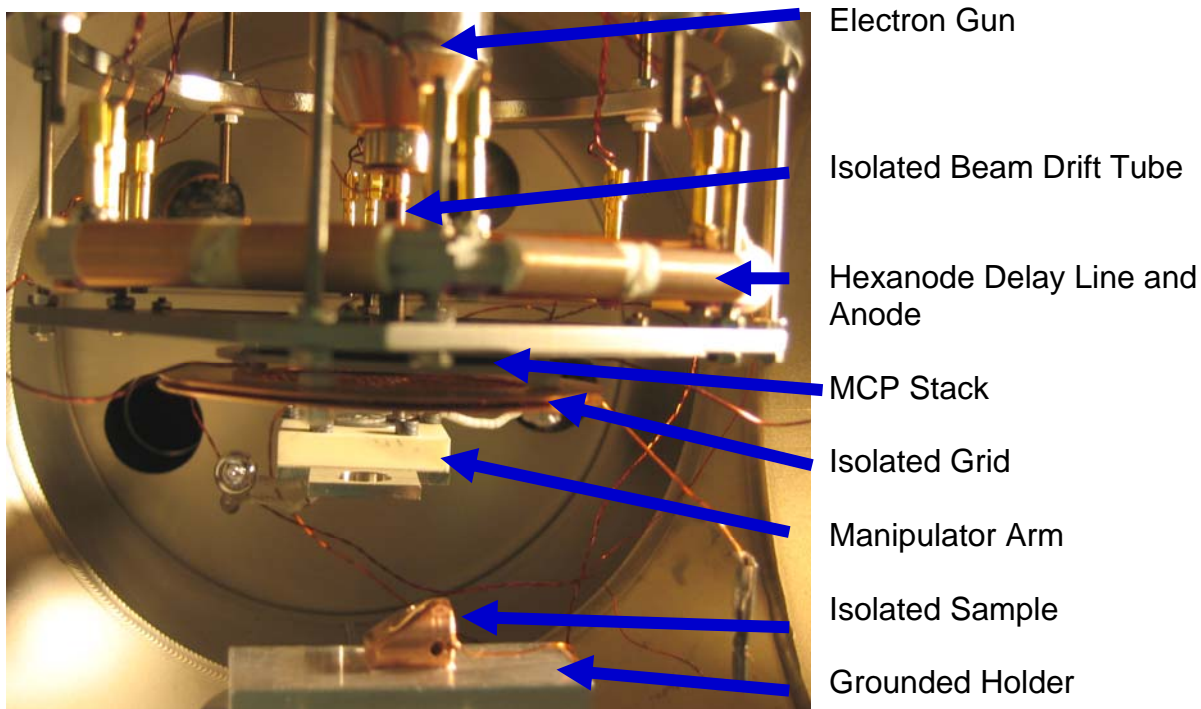Manipulator Arm

Isolated Sample

Grounded Holder

Fig. 1. The internal components of the UNLV SEE Test Stand. The beam drift tube, grid, and sample have been modified in order to be able to perform *absolute* secondary electron emission measurements. Such measurements could only be obtained by pushing the limits of the electron gun beyond manufacturer's specifications to satisfy constraints set by the particle position detector.
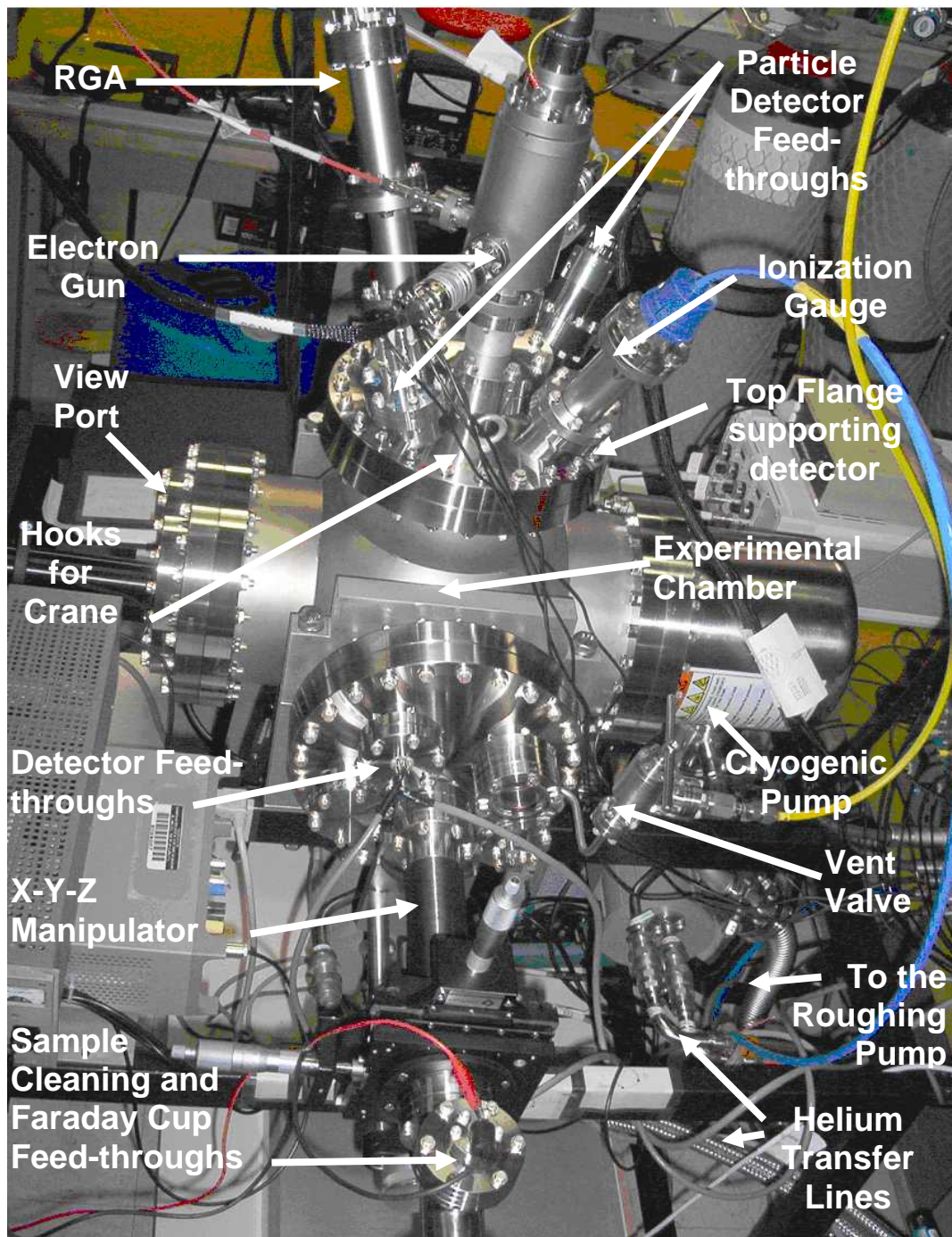
Fig. 2. An external view of the UNLV Secondary Electron Emission (SEE) Test Stand prior to and during the grant period.
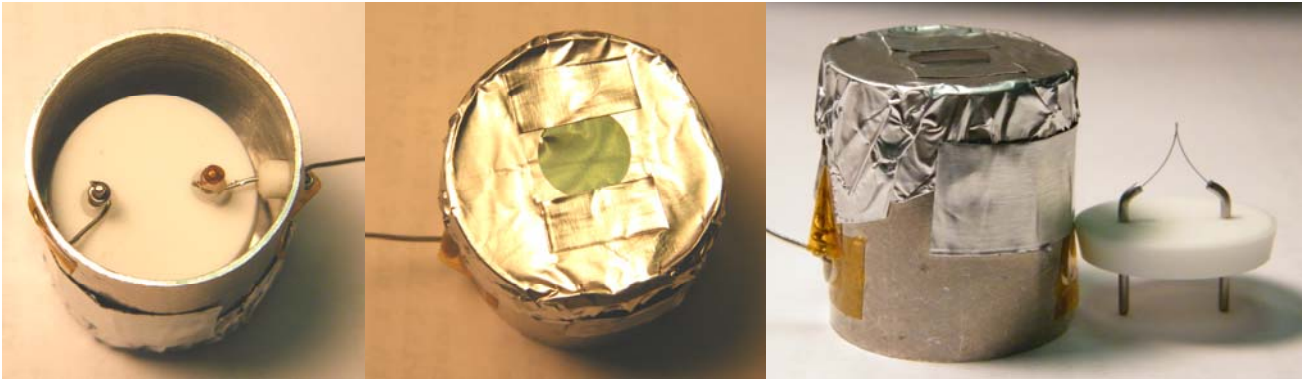
Fig 3. The electron source with filament and optics grade pinhole is displayed.
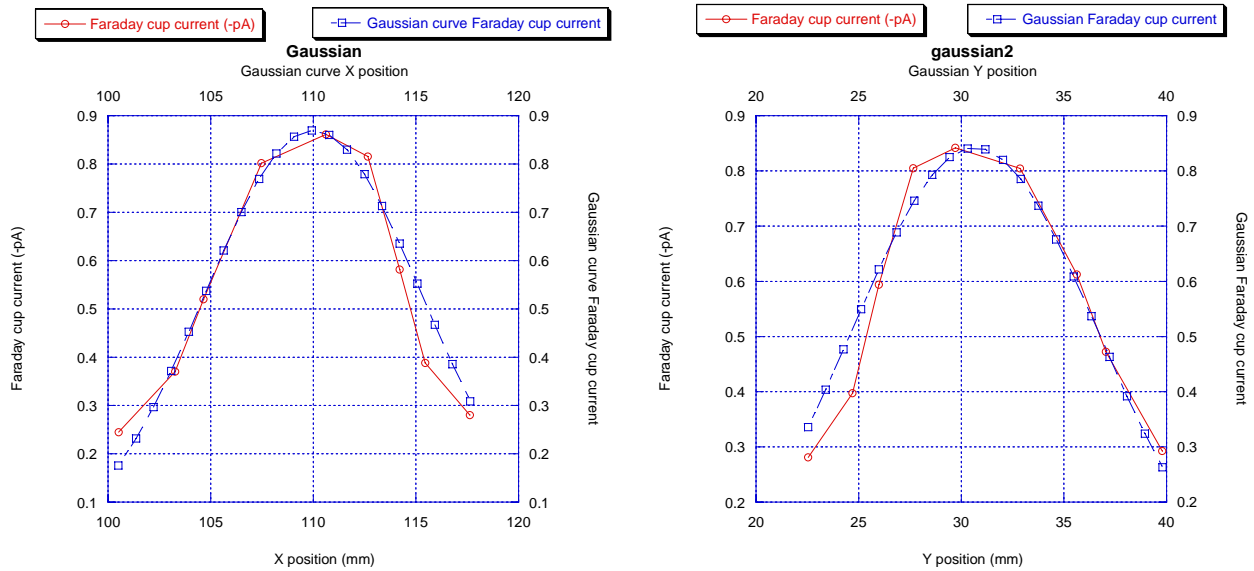

Fig. 4 Current emitted from electron source as collected by a Faraday cup scanned over the source's pinhole in two orthogonal directions. The pinhole diameter is 20 µm. A 2.1 V DC source drives the filament resulting in 2.31 A being supplied to the filament/connecting wire assembly. The Faraday cup is 7 mm from the pinhole.

Absolute measurements are based on careful deductions and inductions, calculations, modeling tools, and careful understanding of equipment limitations (Refer to Garner 2007). It was deemed important to qualify the orientation of the detector relative to target position. This could not be accomplished with confidence based on inferences from the collected secondary electron emission from a target under test since deduction was used to describe the surface properties of the target itself. Another technique was required for validation. It is important to note that the detector orientation is dependent on a number of factors upon assembling the test stand after maintenance and can be easily altered in a number of ways if not careful. Coordinating the detector orientation with respect to the target and computer generated scatter plots is necessary when conjecturing the physics of the surface sample from data. Consequently, an electron source with a fine pinhole aperture was designed to replace the sample and impinging electron beam in order to characterize the detector. Figure 3 displays the UNLV designed and built electron source consisting of a hairpin tungsten filament housed inside an aluminum cylinder. One end of the filament is connected to the aluminum cylinder which is, in turn grounded to the chamber. The top of the cylinder is covered with aluminum foil supporting an optics grade spatial filter with a D=20 micron diameter pinhole. Of the discrete pinhole diameters available to us (15, 20, 35, 50 µm), no electrons were detected from pinholes less than 20 microns. The purpose of the pinhole is to crudely collimate the beam of electrons in a very small region of space. Because of the low filament resistance, the resistance of the wire assembly including chamber ground was measured. The resulting resistance due to wires

10

both internal and external to the vacuum chamber is R_W= 0.141 Ω; the return path from the chamber feedthrough to the location of the aluminum cylinder is R_C=0.065 Ω; and the resultant resistance due to the two filament posts is R_p=0.006 Ω. The total resistance of the connecting wire assembly including filament posts and chamber ground return path is 0.212 Ω. The filament resistance at room temperature measures at 0.069 Ω. Because of the dissimilar metals between the filament and filament posts, small potentials are generated. A typical Ohm meter upon reversing probe positions will yield different resistance readings which includes resistance with negative values. All measurements were made with a BK Precision Bench LCR meter to avoid such erroneous results. In testing the electron source, a 2.1 DC voltage was applied resulting in a filament/connecting wire assembly current draw of 2.31 A. The total resistance of the filament with connecting wire assembly in a thermodynamic equilibrium, T_{Ho}, is 0.91 Ω. The filament resistance at T_{Ho} is R_{fHo}=0.698 Ω. The filament current density was measured with a Faraday cup with aperture radius and area of 0.1 mm and A_{FC} =3.142e-8 m^2 respectively. The current recorded by the electrometer connected to the Faraday cup is as scanned over the pinhole in two orthogonal directions. Figure 4 illustrates an approximate symmetry in polar angle about the pinhole center. Consequently, a Gaussian curve of the form $J_s(r) = J_{os}e^{-\alpha r^2}$ was fitted to the data yielding J_{os}(FCP) [=I_{max}/A_{FC}] =2.8e-5 A/m^2 and α=0.0191e6 m^{-2} [where I_{max}=0.88 pA]. The acronym FCP (Faraday Cup Plane) implies the plane the Faraday cup lies in. The measured cup current divided by the cup area yields the current density at the central location of measurement. The total amount of charge generated by the source is the integration of the modeled Gaussian curve over area yielding

$$I_{so}(T_{Ho}) = 2\pi J_{so}(PHP)\int_{o}^{D/2} re^{-\alpha r^2}dr = 2\pi J_{so}(FCP)\int_{o}^{\infty} re^{-\alpha r^2}dr = \frac{\pi}{\alpha}J_{so}(FCP) \tag{1}$$

where PHP is the pinhole plane. For simplicity, the range of integration over the Faraday cup plane has been extended to infinity since the Gaussian curve decays rapidly as r increases yielding only a small added contribution to the current. Therefore, I_{so}= 4.6 nA DC in a steady state condition.

Based on the characterization of the source at this point and on theory, the operational conditions of the electron source outside of the characterized state may be determined. The physical geometry of the filament is not known and could not be adequately measured without affecting the filament's characteristics. Consequently, using well known resistivity-temperature curves (Fig. 5) and the room temperature resistance, one can deduce the temperature T_H of the filament. At room temperature T_R, a R_{fR}= 0.069 Ω filament resistance was measured. Noting that the DC resistance of a uniform cylindrical parallel plate electrode resistor is R=Lρ/A where L is the length of the resistor, A is the cross sectional area, and ρ is the resistivity, the resistivity at T_H is

$$\rho(T_H) = \frac{R_{fH}}{R_{fR}}\rho(T_R). \tag{2}$$

Figure 5 provides the resistivity-temperature curve for tungsten as measured from two different experimental studies.[5,6] The experimental temperatures range from about 293 ^oK (20 ^oC) to about 3600^oK (3327 ^oC). The melting point of Tungsten is 3410 ^oC. We fitted T.W. Zerda[5] data to a third-order polynomial to yield

$$\rho(T[^oK]) = -2.3953 + 0.024971xT + 2.4734x10^{-6}xT^2 - 9.9652x10^{-11}xT^3 \quad [\mu\Omega - cm] \tag{3}$$

Correlation Coefficient CC = 1 Pearson Test

11

where T is in degrees Kelvin and $\rho(T)$ is in $[\mu\Omega - cm]$. A correlation coefficient CC=1 (Pearson test) implies that the curve fit is optimal within the temperature range displayed. The correlation coefficient varies between 0 and 1 inclusive. At T=20 °C, the commonly accepted resistivity of Tungsten ranges between 5.5 to 5.65 $\mu\Omega$-cm. At T_R, the resistivity of tungsten based on Zerda's[5] tests is 5.65 $[\mu\Omega - cm]$ whereas Eq. (3) predicts a value of 5.13 $[\mu\Omega - cm]$. Using the former value, the resistivity at the filament temperature of the electron source based on the characterization study is T=T_{Ho} for a hot tungsten resistance of R_{fHo}=0.698 Ω is $\rho(T_{Ho})$ =57.16 $[\mu\Omega - cm]$. From Eq. (3), the temperature of the hot filament generating an electron source current of I_{so}= 4.6 nA is T_{Ho}= 2015 °K.
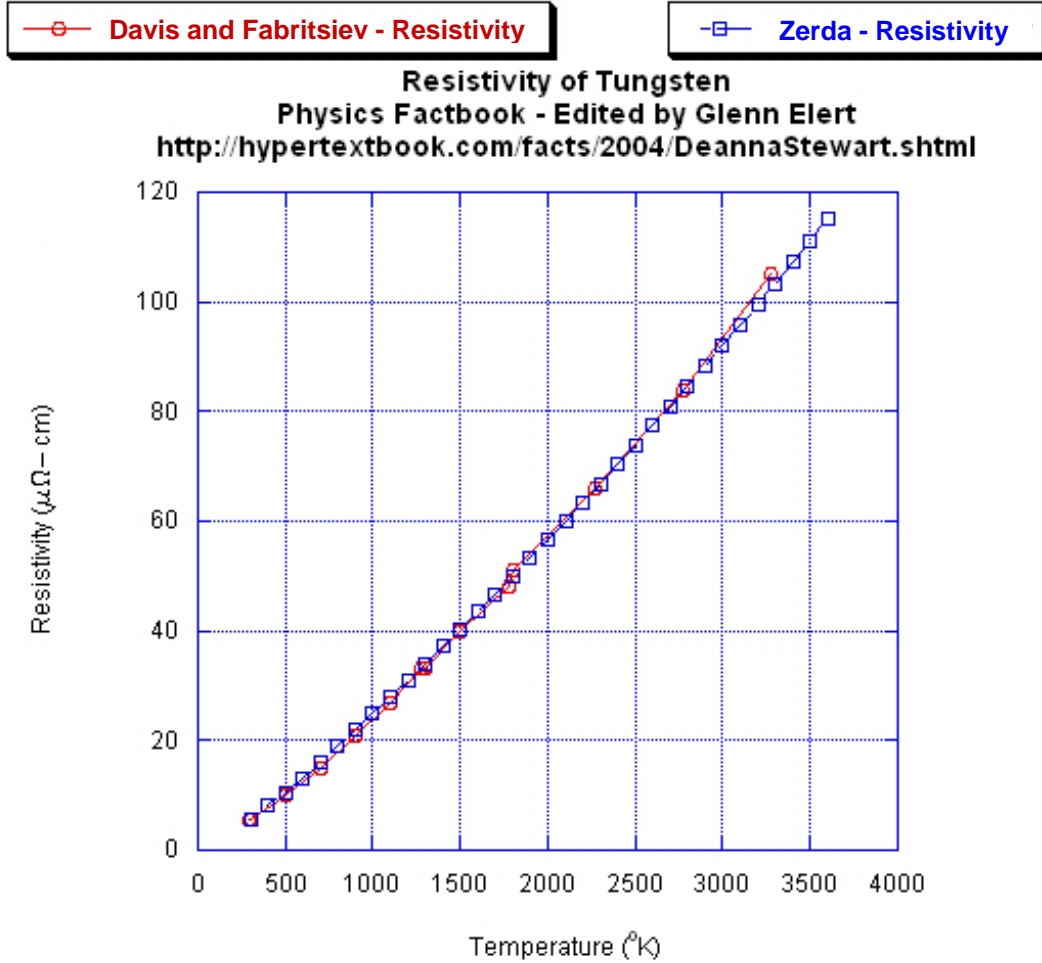

Fig. 5. Displays the resistivity of tungsten from room temperature to its near melting point based on two different experimental results.[5,6] The melting point of Tungsten is 3683 °K (3410°C).

The current density emitted at the filament surface is governed by the Richardson-Dushman equation

$$J_e(T) = A_o T^2 e^{-\left(\phi_m / KT\right)} \quad [A/cm^2]$$

(4)

where A_o is the thermionic emission constant (=60 $[A/(cm^2 - K^2)]$ for tungsten), ϕ_m is the work function (=4.5 eV for tungsten), T is the filament temperature in °K, and K is the Boltzmann constant (=8.63x10⁻⁵ eV/°K). We assume that the distribution of charge (not the magnitude of charge) generated by the emitter is independent of temperature. Therefore, the total source current emitted by the electron source due to thermionic emission with source orifice is

12

$$I_s(T) = \beta J_e(T) = \tilde{\beta} T^2 e^{-\left(\phi_m/KT\right)} \tag{5}$$

where β takes into consideration the aperture geometry and the probability of the electrons passing through the orifice. Knowing the source current at one temperature, one can deduce the current at another temperature by examining the ratio of currents. Consequently, the source current at any temperature within the limits of the validity of the relation characterizing thermionic emission yields

$$I_s(T) = I_{so}(T_{Ho}) \left(\frac{T}{T_{Ho}}\right)^2 e^{-\frac{\phi_m}{KT_{Ho}}\left(\frac{T_{Ho}}{T}-1\right)} \tag{6}$$

where the temperature T may be determined from the measured filament voltage and current with the assistance of Eqs. (2) and (3). The experiments conducted below to characterize the particle position detector, are based on a 3 V filament bias drawing 2 A of current. The electron source filament resistance, resistivity, temperature, and source current are respectively, R_{fH}=1.29 Ω, $\rho(T)$ =105.5 $\left[\mu\Omega - cm\right]$, T =3355 $^{\circ}$K, and $I_s(T)$= 0.39 mA. The source current is very high.

Figure 6 provides a typical dark count baseline. Two separate dark count studies have been conducted with nearly the same result. A vacuum pressure of 7.6e-8 Torr was achieved. The MCP front, MCP back, anode, and reference bias voltages are 300V, 2.2 kV, 2.2 kV, and 2.5 kV respectively. The associated currents in sequence are 0.318 mA, 0.012 mA, 0 mA, and 0.001 mA. The dark count over a three minute span yielded 7368 counts or, equivalently, about 41 counts/sec. The MCP does have a lifetime associated with it. Over time, the MCP degrades and one has to increase the bias voltages within limits to achieve the same level of detector sensitivity relative to an earlier point in its lifetime. We use the dark count as a means to monitor the sensitivity of the MCP. The MCP bias voltage is adjusted until the present dark count is comparable to that in an earlier experiment. Typically, this adjustment is not necessary over short durations of time such as months assuming that one is careful with the detector. Over an eight month period or when accidental high intensity exposure results, bias adjustments can be expected.
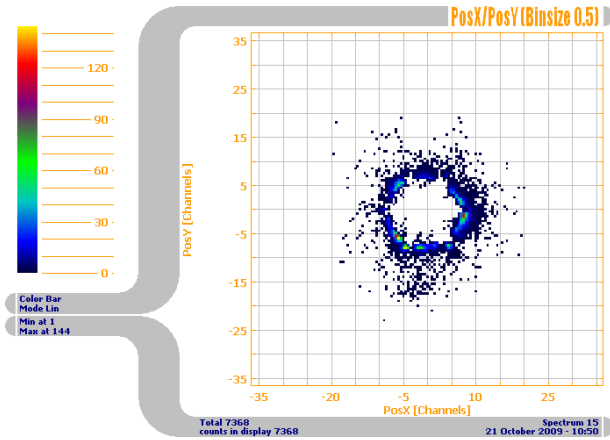

Fig. 6. Dark count study prior characterizing the detector with filament source. The total count over a three minute span is 7368.
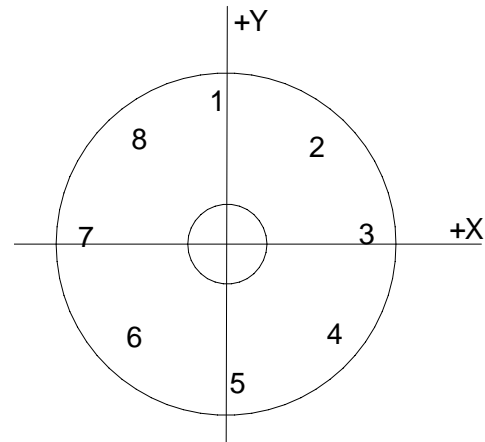
Fig. 7. Schematic of the detector. Positions 1-8 identify the location of the source stimulating the detector. These locations correspond with the test numbers provided in Figs. 8 and 9.
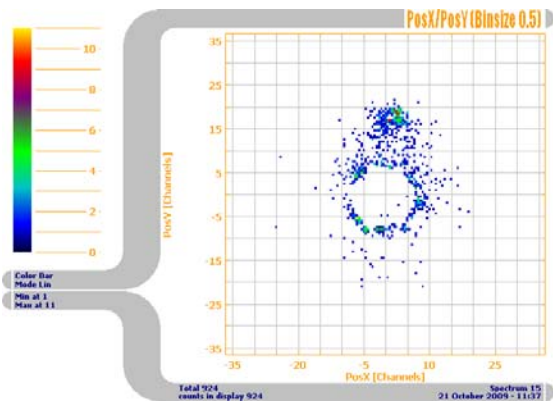
Test 1 (924 Counts in 7.94 s)
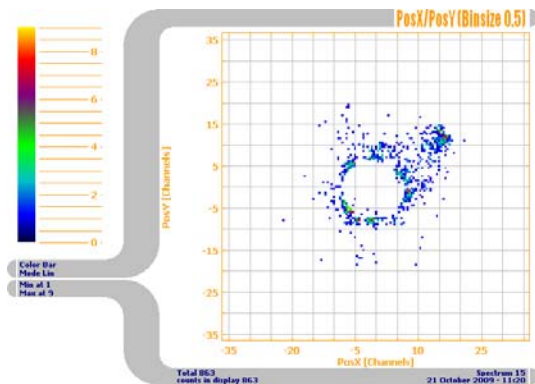
Test 2 (863 Counts in 8.37 s)
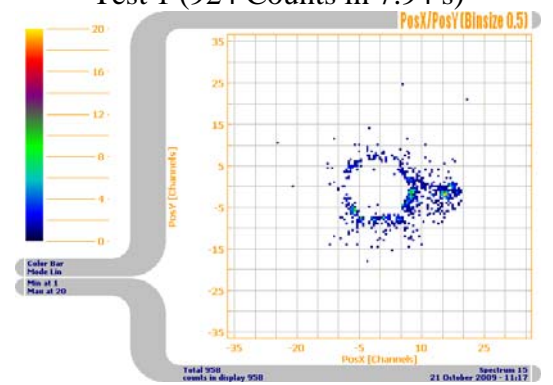
Test 3 (958 Counts in 7.31 s)
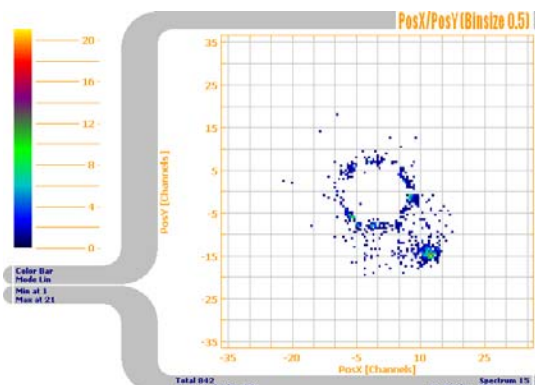
Test 4 (842 Counts in 7.55 s)
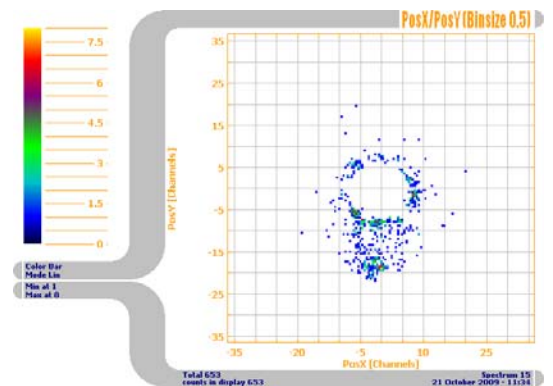
Test 5 (653 Counts in 7.20 s)
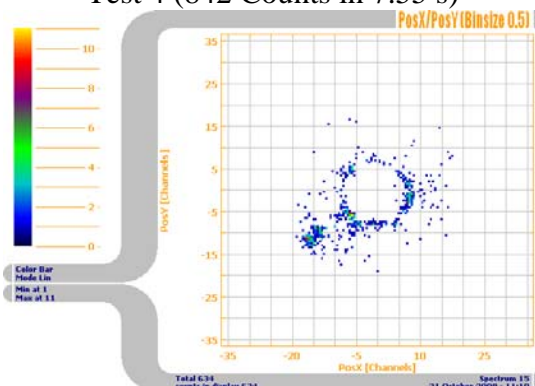
Test 6 (634 Counts in 7.14 s)
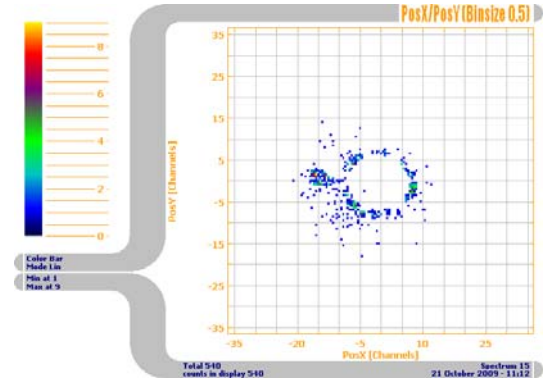
Test 7 (540 Counts in 6.46 s)
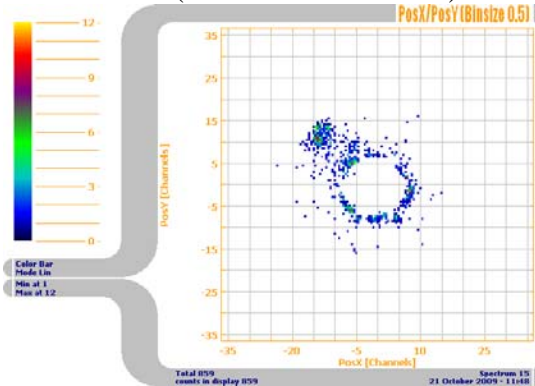
Test 8 (859 Counts in 7.99 s)

Fig. 8 Raw test data corresponding with illuminated regions depicted in Fig. 7.
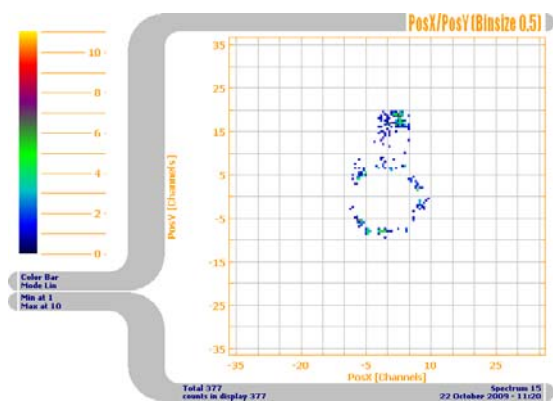
Test 1 (377 Counts in 7.94 s)
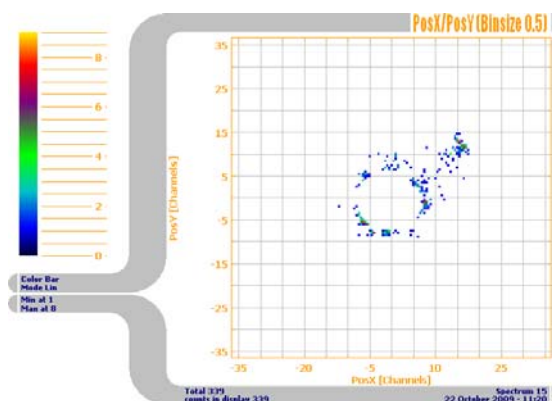
Test 2 (339 Counts in 8.37 s)
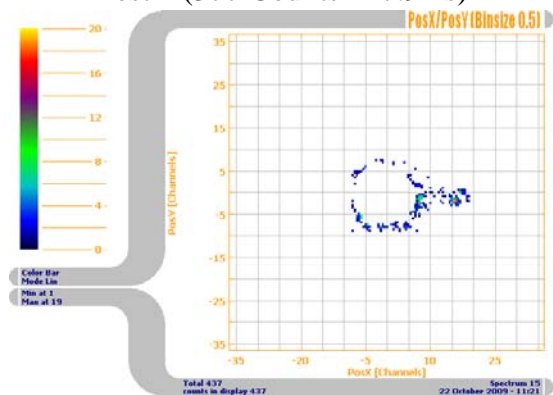
Test 3 (437 Counts in 7.31 s)

Test 4 (398 Counts in 7.55 s)

Test 5 (238 Counts in 7.20 s)

Test 6 (247 Counts in 7.14 s)

Test 7 (216 Counts in 6.46 s)

Test 8 (399 Counts in 7.99 s)

Fig. 9 Processed data corresponding to Fig. 8. One count is subtracted from each bin containing one or more electrons.

Figure 7 illustrates the relative alignment of the electron source with respect to the particle position detector. The approximate distance between t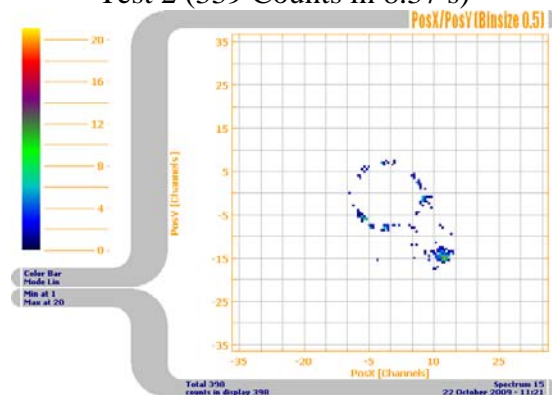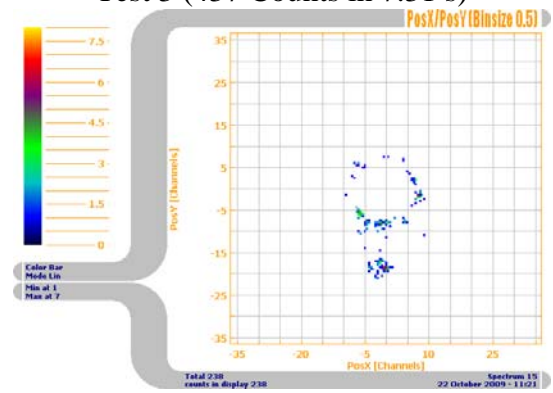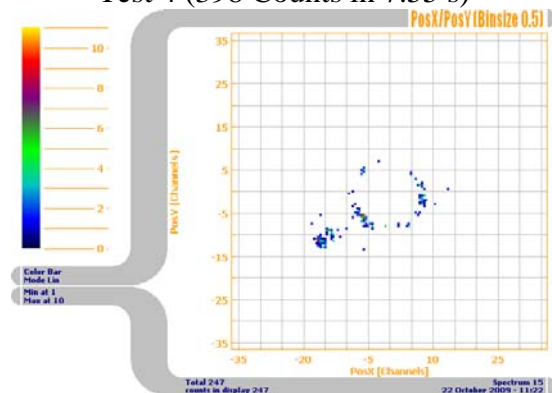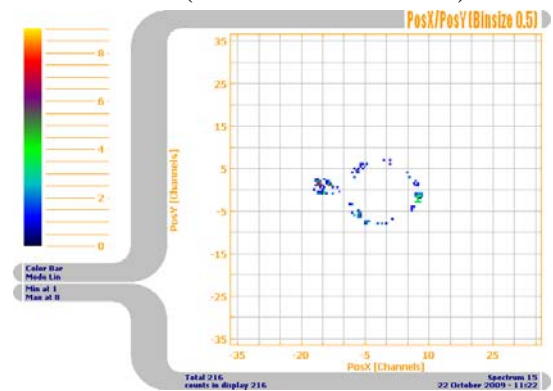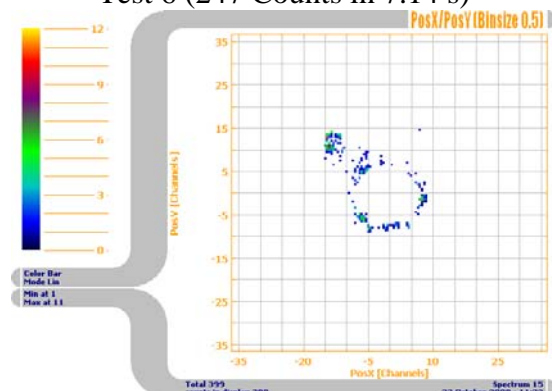he pinhole of the electron source and the grid is about 0.5 cm. The numbers 1-8 identify the location being illuminated with the electron source. The location number is directly associated with the test number in plots that follow. Because the source current is so high, the source is on only for a brief moment during the time when data is taken. The data is monitored in real time providing feedback when to turn the source off. As the experiment commences and data is taken, the filament of the electron source is turned on. Consequently, it takes time for the filament to heat up and for the electrons to populate the electron source cavity. Many of the electrons are lost to the cavity wall which is grounded. A small number find the pinhole and escape the electron source cavity. The data displayed in Fig. 8 clearly shows the position of the captured electron cluster of the source. Good agreement is shown with respect to Fig. 7 allowing for alignment between source, detector, and computer generated display. Further, the data in Fig. 8 show no signs of detector saturation or significant false counts.

The data in Fig. 9 is processed by subtracting one from each bin containing one or more electrons. The purpose is to examine the location of the maximum concentration of charge especially since the dark count is within an order of magnitude compared to the electron count recorded by the detector with the electron source on. Since the dark count is typically a random event except near regions where discharge results are due to device imperfections, one should expect to be able to remove many of the electron counts not associated with the electron source. The electron beam is clearly distinguished and demarcated from the dark count. Qualitatively, the illuminated portion of the particle position detector agrees well with proximity. Further, the electron bunches are tightly formed. In each case above, a significant charge distribution lies around the perimeter of the central hole in the particle position detector where the beam drift tube exists. This is due to imperfections resulting from a centered hole in the particle position detector and grid to allow the primary beam electrons to reach the sample under test.

The above study was performed based on the transient nature of the source allowing for just enough charges to leave the electron source to make the measurement prior to the time the source reaches its large steady state current condition. The time constant was long enough that measurements could be taken without saturating the detector. In the future, a similar study will be performed on a quantitative steady state basis to further verify and fine tune theoretical predictions for *absolute* measurements. Based on Faraday cup measurements and theory, the source current directed towards the detector will be adjusted to levels low enough for continuous detector exposure. The source current will be known or, if too small to measure, will be deduced by its operating conditions. As indicated in Garner's thesis (UNLV 2007), the copper grid and the MCP blocks a fraction of the incident beam from being detected. Based on past works, we have determined the number of electrons that will be lost to the grid and the MCP. The number of electrons per unit time that will reach the detector is predicted by

$$I_D = (1 - GridLoss)(1 - MCPLoss)I_s \tag{7}$$

where *GridLoss* and *MCPLoss* represents the fraction of electrons lost to the grid and the MCP. The *MCPLoss* (=0.52) is based on the calculation relating the ratio of the total MCP area minus pore opening area to the total MCP area. The *GridLoss* is based either on the measured grid current $(I_g = I_s \times GridLoss)$ or on grid geometry. In terms of grid geometry, the *GridLoss* (=0.82) is the empirical effective area blocked by the grid relative to the total area. Empirical studies are performed by suitably flooding the region with electrons and visually examining the data for void of electrons revealing the pattern of the grid. In a future study, we will use the electron source in a steady state mode while monitoring grid currents and detector counts to understand the grid losses and MCP losses with more accuracy thereby fine tuning the properties of the machine.

III. Modeling Studies

Magic Simulation

      The MAGIC code has been used to simulate experiments conducted in the UNLV SEE Test Stand. With the aid of ATK Mission Research Inc., we were able to simulate picoampere electron beams colliding in a metallic target on nanosecond time scales. For a statistically valid simulation, tens of thousands of individual particle runs with random variable seed condition are needed to characterize the secondary electron emission physics based on a Monte Carlo calculation in the target. Alternatively, one could argue that one charge could be divided into thousands of identical charges each with the same charge to mass ratio. The average center of mass of the charge ensemble would preserve the motion of the actual single charge. The sub-charges would now characterize the probability that a charge will exhibit a particular trajectory. This probability will be approximately equivalent to the probability obtained by evaluating thousands of individual charge particle trajectories with a random number generator. ATK has revised the code to allow UNLV to characterize grid current loss and detector currents (not MCP loss at this time) in the simulation.
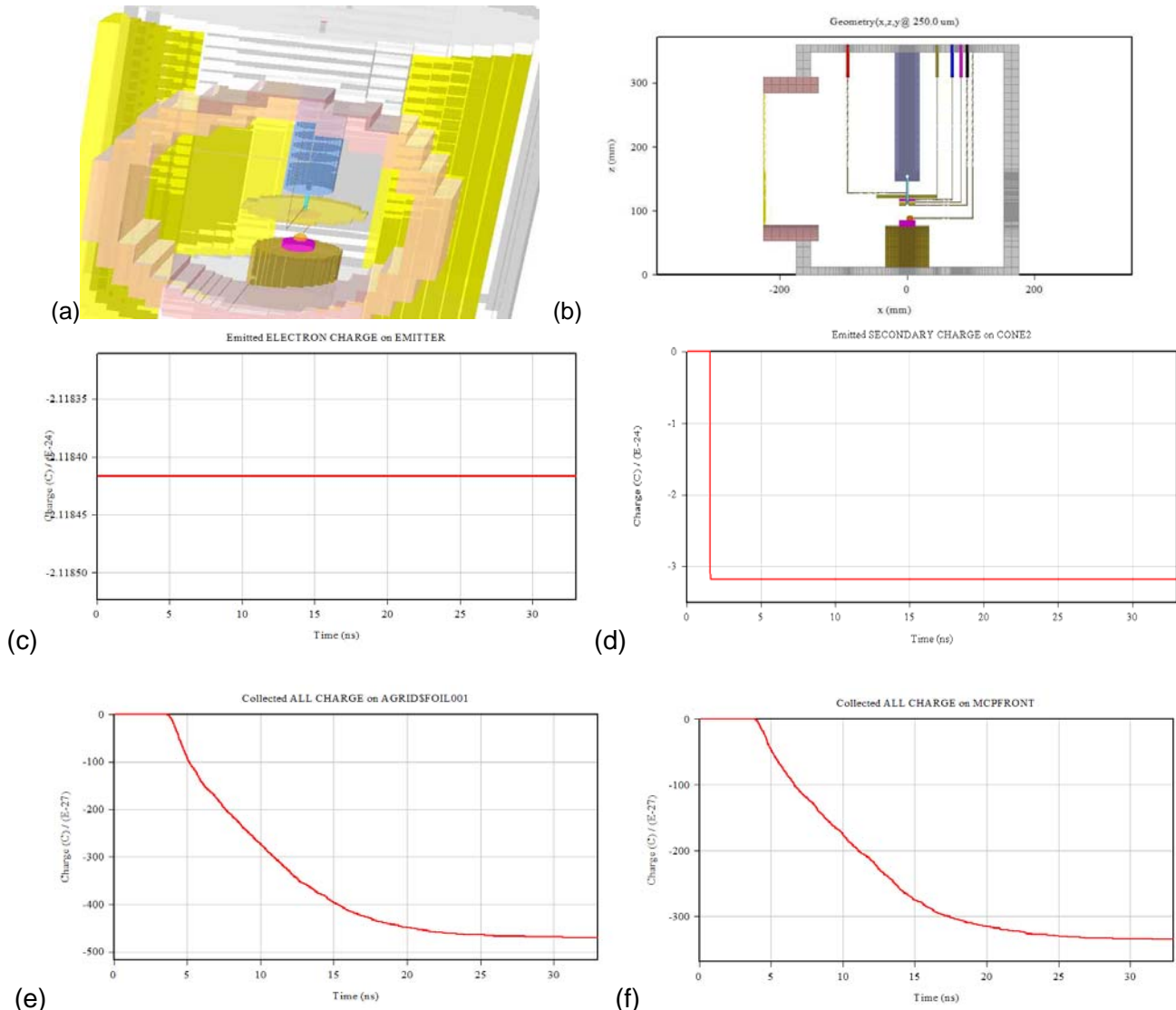

Fig. 10 a-e A composite of the SEE Test Stand is illustrated in a) three-dimensions and b) two-dimensions. All entities including wires connectors and ports are contained in the simulation. The c) total source emitted charge (2.11842e-24 C), d) the total sample emitted secondary electrons (3.19e-24 C) e) total grid (470e-27 C), and f) microchannel plate charge (350e-27 C) are monitored.

17

Figures 10a,b display a three dimensional and two dimensional picture of the SEE Test Stand respectively. Because of the close proximity of the components and the experimental constraints on geometry, significant effort was placed into scaling all of the major components into the simulation. Special care was taken to make sure that the simulation was in a DC bias state prior to releasing the electrons generated by the gun. To obtain one steady state condition (without electron beam) requires about three weeks to a month of real time to reach a steady state condition of roughly 1 μs simulation time. Once obtained, the final steady state conditions were used as initial conditions for the electron beam simulations. The simulation presented in Figs. 10c-f, models the experiments performed in the SEE Test Stand. A 75 μm diameter, 8.5 ps pulsed, 500 eV, 0.5 pA electron beam is released by an emitter at the exit end of the beam drift tube in the simulation. The pulsed electron beam is composed of 100,000 equally weighted particles (sub-electrons) to simulate the statistical nature of the emission. The secondary electron yield assigned to the sample is 1.5. Figures 10c,d show that the total charge emitted by the emitter and the secondary electrons generated by the sample are respectively about 2.118e-24 C and 3.19e-24 C. All charge generated by the emitter representing the primary electron beam collides with the sample. The ratio of the secondary electrons generated at the sample to the incident primary beam electrons is ~1.5 as expected. *Normalizing the total charge collected by the electron grid and microchannel plate to the total primary number of electrons in the primary electron beam* (Refer to Fig. 1 and Figs. 10e,f), the probability that the grid and microchannel plate will intercept a charge is 22% and 16.5% respectively. It is noted that MAGIC handles the physics of the wire grid based on a transparency probability as defined by the user. Based on the ratio of total pore area to microchannel plate area, the fraction of charge lost to the MCP is *MCPLoss*=0.52. Therefore, MAGIC predicts that the detector will observe about 7.92% of the electron gun emitted charges. In the same manner *based on the number of secondary electrons generated*, the percent of secondary electrons collected by the wire grid, MCP, and lost to the system (e.g., vacuum walls, holders, etc.) are respectively 14.7%, 11%, and 74.3%. For a typical experimental emission test, a 100 ms pulsed, 0.5 pA, 500 eV electron beam is generated within a 75 μm diameter beam. Consequently, about 312,500 electrons are released by the electron gun. Typically, the number of electron counts recorded in 100 ms is between 500 and 1500 electrons at a 30° grade from a reasonably polished copper (and niobium) sample. Choosing a middle conservative count of 1000, the percentage of charge detected with respect to that generated by the electron gun is 0.32%. Here we assumed a rectangular pulse with respect to time. In experiments, the electron distribution is not rectangular with time. Therefore, we allow for a triangular distribution which increases the percentage by about 2 to 0.64%. The maximum secondary electron yield for copper and niobium is typically 1.3 at 600 eV and 1.2 at 375 eV respectively. The range of the primary beam kinetic energy at impact for secondary electron yields greater than one for copper and niobium are respectively 200 eV to 1500 eV and 150 eV to 1050 eV.[7] Therefore, relaxing the SEY condition in MAGIC from 1.5 to 1.3, based on ratios, the MAGIC will observe about 6.86%. MAGIC predicts nearly one order of magnitude more charge to be detected as compared with experiments. This is reasonably close since MAGIC is only provided with the bulk material, the material geometry, and a single user provided SEY value (in our case). MAGIC has the ability to incorporate known energy distributions which we have not used. Further, curved lines and surfaces are generated with orthogonal lines and planes having discrete step changes to approximate the curve. The curved surface placed in front of the primary beam may not appear graded to the impinging electron. Look-up tables, surface physics, and/or generic yield curves contained in most PIC codes are based on high energy physics which is not necessarily valid at the experimental energies of interest. As a final note, low energy primaries (<500 eV) tend to generate more true secondary electrons than high energy primary electrons.

Monte Carlo SEE Code

Typically, low energy primary electrons (energy range between 10 eV and 1 keV) have a greater probability in generating **true** secondary electrons with substantial yields based on material properties and surface physics. The number of low energy primaries and the secondaries they

generate is small enough that a detailed collision history is possible with today's computer power. The single scatterer approach is a microscopic study of the detailed collision history of the particles. Therefore, microscopic physics driving the scattering process is intact. This allows one to study the surface physics in monolayers (microscopic scale) since microscopic physics is intact.
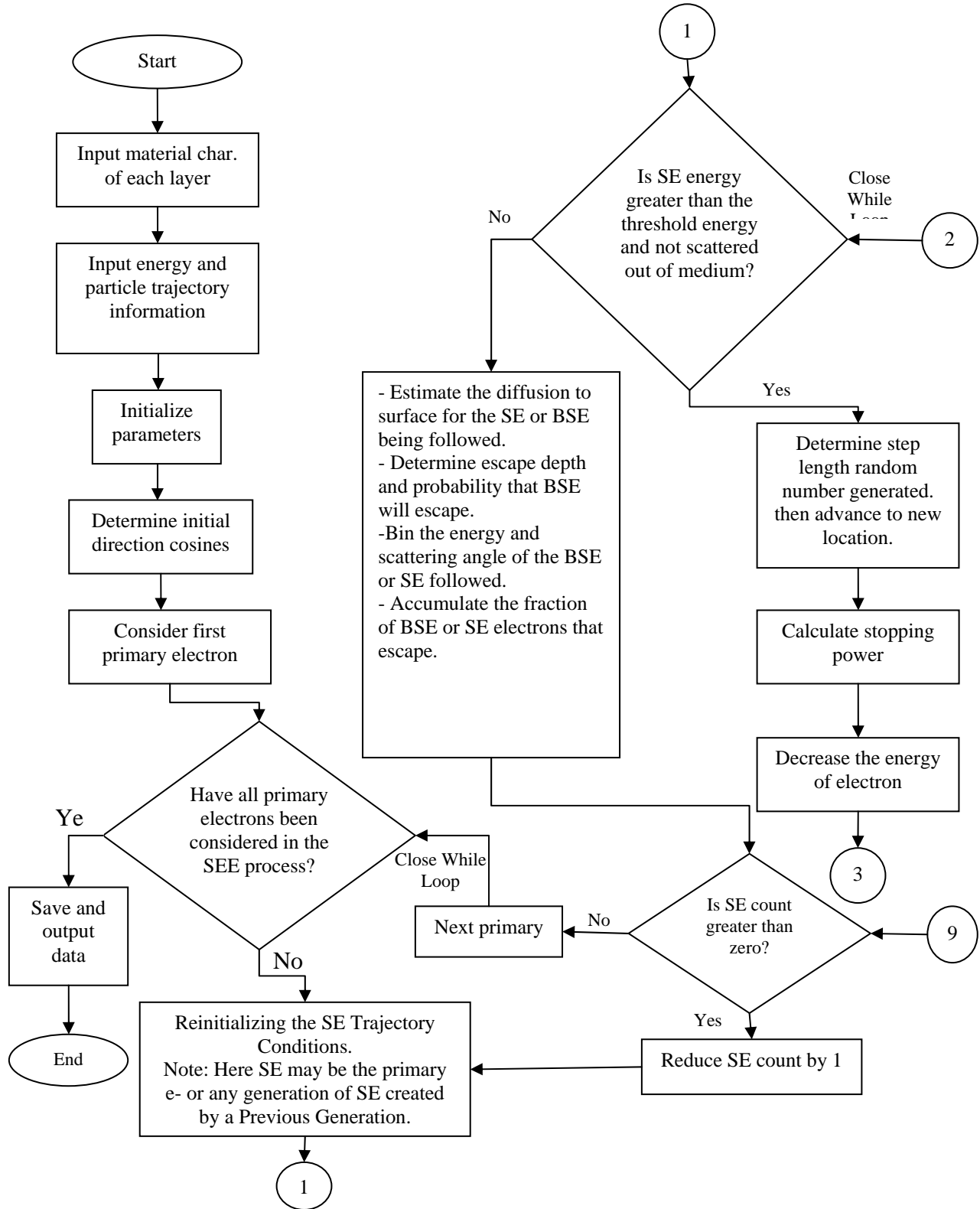
Other more involved codes use a macroscopic approach to model secondary electron emission. For example, an integrated tiger series is used based on an averaging technique born at the time when discrete calculations where time consuming. This is a plural scattering or condensed history approach. This series was designed to deal with collision cascades generated by keV and MeV charged particles since they generate a very large number of secondary electrons. This approach does not follow the detailed collision history (condensed history). Consequently, one loses insights on the microscopic physics that drives the macroscopic processes. Current codes such as the Large Scale Plasma (LSP) code and possibly MAGIC use this macroscopic approach or some similar approach to model low energy secondary electron emission physics. The extrapolation and the physics behind the model providing the extrapolation are in question when extended to a low energy primary electron or a low energy secondary electron acting as a primary.

Historically the implementation of MC methods to calculate SEE yields relied heavily on empirically determined approximations which were reasonable for high energy primary electrons but which are inappropriate at low energies. These approaches attempted to lump all the inelastic processes in a collision cascade into a single energy dependent loss rate function (called the stopping power). This approximation is analogous to a net viscous drag. While this works very well to characterize the history of a primary, it provides no direct information to allow a calculation of the secondary electron (SE) production rate. Moreover, at low energies the interactions are no longer well described by the classical approaches developed early in the last century.

The general Monte Carlo (MC) method presumes to estimate the behavior of a large ensemble based upon a random sampling of a few. The case of interest here is to determine the number of electrons emitted from a surface for every electron striking the surface. In addition, we seek the angular distribution and energy of the emitted electron as a function of the angle and energy of the primary electrons.

When an electron strikes a target it can penetrate hundreds of monolayers and can undergo multiple collisions with the constituent nuclei and electrons. The electron slows as it moves, loosing energy to the medium, it is scattered (changes direction), and eventually it is either scattered out of the medium (is emitted) or it comes to rest (i.e., becomes thermalized). It is a matter of chance that determines the host nuclei involved in these collisions, host electrons struck, and the incident angle of collision. In order to apply the Monte Carlo to electron scattering, we estimate the probability distributions for each type of event that can occur and use random numbers to select a sequence of scattering events that, on the average, produce a distribution that agrees with our expected probability distributions. We then follow the progress of an electron through a target while requiring that, at each step of the way, the results are consistent with our best models of physical reality, i.e., the physics. The probability distributions for the scattering of the electron into some angle by a particular type of nucleus depends upon the apparent cross section of that nucleus, the number density in the target, and the energy of the incident electron.

Secondary Electron Emission Monte Carlo Code – Simplified Flow Chart

```
                                                              ( 1 )
                                                                │
        ( Start )                                               ▼
           │                                            ◇ Is SE energy
           ▼                                              greater than the
┌──────────────────────┐                          No      threshold energy      Close
│ Input material char.  │ ◄──────────────────────────     and not scattered      While
│   of each layer       │                                 out of medium?         Loop     ( 2 )
└──────────────────────┘
           │
           ▼
┌──────────────────────┐                                                       Yes
│ Input energy and      │                    ┌──────────────────────────┐        │
│ particle trajectory   │                    │ - Estimate the diffusion to│       ▼
│   information         │                    │ surface for the SE or BSE │  ┌──────────────────────┐
└──────────────────────┘                    │ being followed.           │  │ Determine step        │
           │                                │ - Determine escape depth  │  │ length random         │
           ▼                                │ and probability that BSE  │  │ number generated.     │
┌──────────────────────┐                    │ will escape.              │  │ then advance to new   │
│   Initialize          │                    │ -Bin the energy and       │  │   location.          │
│   parameters          │                    │ scattering angle of the BSE│ └──────────────────────┘
└──────────────────────┘                    │ or SE followed.           │        │
           │                                │ - Accumulate the fraction │        ▼
           ▼                                │ of BSE or SE electrons that│ ┌──────────────────────┐
┌──────────────────────┐                    │ escape.                   │  │ Calculate stopping    │
│ Determine initial     │                    └──────────────────────────┘  │   power              │
│ direction cosines     │                                                   └──────────────────────┘
└──────────────────────┘                                                             │
           │                                                                         ▼
           ▼                                                              ┌──────────────────────┐
┌──────────────────────┐                                                  │ Decrease the energy   │
│ Consider first        │                                                  │   of electron        │
│ primary electron      │                                                  └──────────────────────┘
└──────────────────────┘                                                             │
           │                                                              ( 3 )       │
           ▼                                                                          ▼
     ◇ Have all primary                          Close While          ◇ Is SE count
       electrons been                              Loop                  greater than     ( 9 )
Ye     considered in the   ◄──────────────  ┌───────────────┐   No       zero?
       SEE process?                          │ Next primary  │ ◄──────
  │                                          └───────────────┘
  ▼            No                                                          Yes
┌──────────┐     │                                                          │
│ Save and  │     ▼                                                         ▼
│ output    │  ┌────────────────────────────────┐              ┌──────────────────────┐
│ data      │  │ Reinitializing the SE Trajectory│ ◄───────────│ Reduce SE count by 1 │
└──────────┘  │ Conditions.                     │              └──────────────────────┘
  │           │ Note: Here SE may be the primary│
  ▼           │ e- or any generation of SE created│
( End )       │ by a Previous Generation.        │
              └────────────────────────────────┘
                             │
                             ▼
                           ( 1 )
```
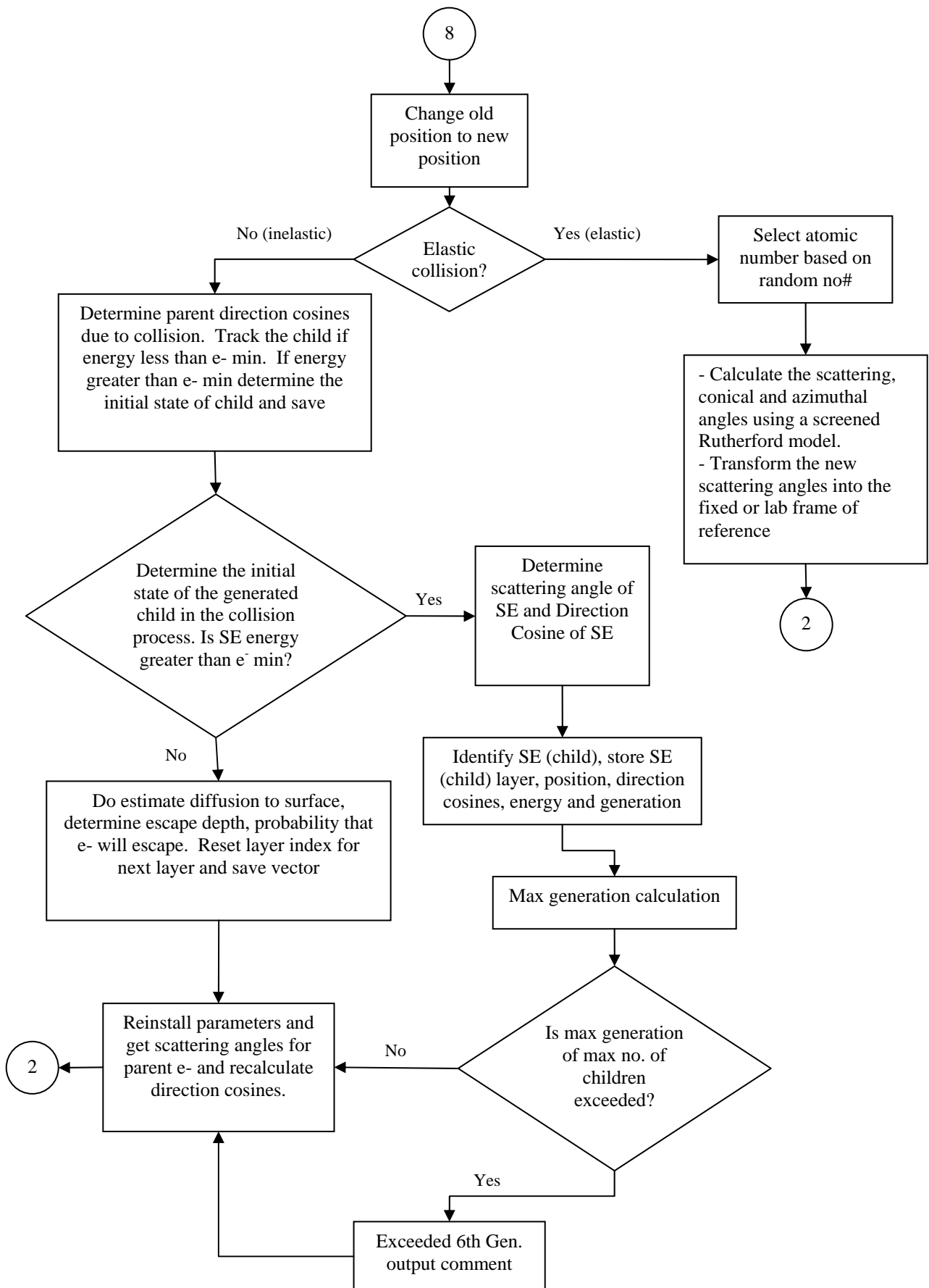
20

(8)

Change old position to new position

Elastic collision?

No (inelastic) / Yes (elastic)

Select atomic number based on random no#

- Calculate the scattering, conical and azimuthal angles using a screened Rutherford model.
- Transform the new scattering angles into the fixed or lab frame of reference

(2)

Determine parent direction cosines due to collision. Track the child if energy less than e- min. If energy greater than e- min determine the initial state of child and save

Determine the initial state of the generated child in the collision process. Is SE energy greater than e⁻ min?

Yes

Determine scattering angle of SE and Direction Cosine of SE

No

Do estimate diffusion to surface, determine escape depth, probability that e- will escape. Reset layer index for next layer and save vector

Identify SE (child), store SE (child) layer, position, direction cosines, energy and generation

Max generation calculation

Reinstall parameters and get scattering angles for parent e- and recalculate direction cosines.

(2)

No

Is max generation of max no. of children exceeded?

Yes

Exceeded 6th Gen. output comment

22

Fig. 11. Flow chart of the UNLV SEE code employing a single scatter approach to study the collision cascade of a primary electron and all generations of charge that the primary and the generations of secondary's create. The current code is written in C++.

Although not within the scope of the funded research, it was deemed important that some effort be placed in surface/bulk modeling of the collision cascade between the primary electron and the target material. As a follow-up on research efforts prior to this grant but associated with the grant (Refer to final report for AFOSR grant number FA9550-05-1-0284.), a detailed flow chart has been developed for the UNLV modified, Monte Carlo Secondary Electron Emission code.   Refer to Fig. 11. The original code was developed by Dr. David Joy for scanning electron microscopy studies allowing for the study of the *entire* collision process using the single scatterer approach; a microscopic technique. Dr. Joy's intent was to replace computer intensive calculations with enough physics to characterize approximately the surface physics of materials in an expedient manner. This allows for the incorporation of other physics and more complex geometry into the code to characterize realistic materials. Because the code was originally based on high energy physics, a low energy electron limitation exists. Interest exists to incorporate low energy physics into the code either based on an effective classical plasma model or based on a quantum mechanical model. UNLV has enhanced the code to handle rigorously multiple layers of multiple atomic or molecular components as thin as a monolayer. Such an arrangement allows for the study of the surface physics of materials supporting multiple monolayer coatings of different materials. The code finds application to novel cathode and anode studies and material studies for high power microwave devices especially those devices employing a high vacuum environment with very tight tolerances between the beam and neighboring structures.

IV.   Highlights of SEE from a Warm Metal Sample

Secondary electron emission experiments were performed from a warm metal sample as the sample cooled (transient cooling). The details of the experimental setup may be found in the ICOPS 2009 slides provided in Appendix A. Probing a buffered chemical polished niobium sample aged for four years in atmosphere with a low energy, low current electron beam, we have been able to separate what we believe are the backscattered and "true" secondary electrons. Figure 12 provides an artist's view of the modified SEE Test stand allowing for microwave induced heating/cooling studies. The copper waveguide terminated with a short on the left side of each figure has a section on the bottom of the waveguide that is removed. This waveguide section is lowered over the target sample supporting an electrically and thermally conducting plate. Once a good electrical short is attained, a pulsed 1 kW, 9 GHz, 6% duty cycle (100 kHz pulse repetition frequency, 600 ns pulse width) microwave source drives a TE_{10} mode in a shorted waveguide with 4cm x 2.3cm broadwall aperture that covers and heats a portion of the thermal copper storage plate surface with sample extending into the waveguide. Suitable thermal insulator materials were used to control the cooling time constant. The system was designed to have a rather long thermal time constant in cooling mode. (Refer to Garner's Thesis, UNLV 2007.) The waveguide is removed and the electron gun is fired at predetermined times while the sample cools to room temperature.
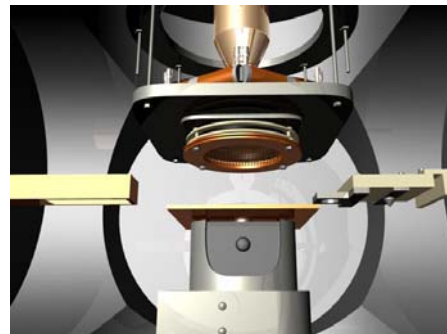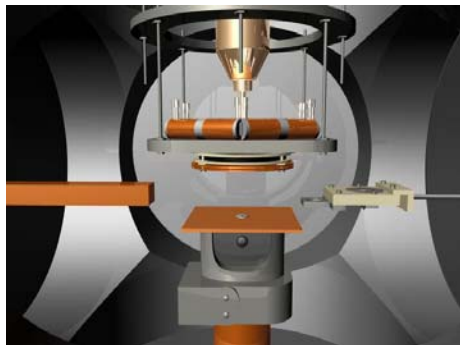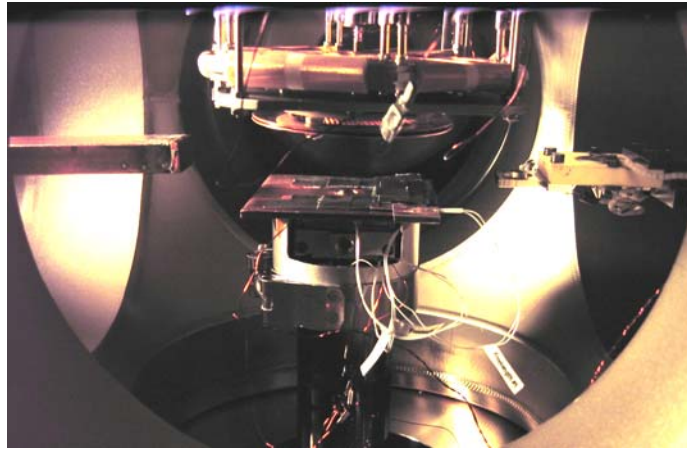
Fig. 12 Both an artist's perception of the UNLV SEE Test Stand and the actual test stand for warm metal experiments. The thermal copper storage plate and sample are shown in each picture.
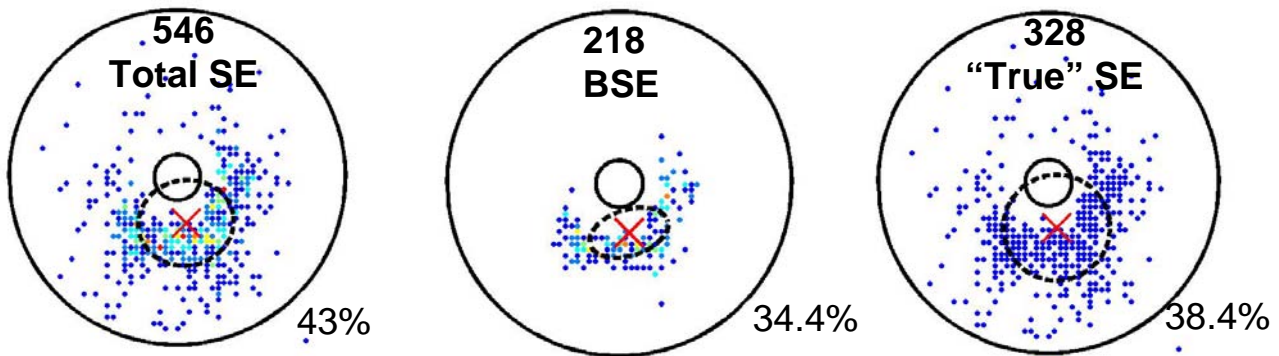

Fig. 13 Typical secondary electron emission results from niobium at 360 $^\circ$K (total count 546) separated into its backscattered emission (count 218) and "true" secondary emission (328 count) components. The dashed line with centralized X displays the mean location of the secondary electron cluster and a two-dimensional standard deviation (elliptical) area about the mean. The listed percentage is the percent of the total captured electron type contained within the ellipse for that electron type. Used as a relative measure, if the circumference of the two-dimensional standard deviation area is circular and the distribution of captured electrons is Gaussian, the number of captured electrons in the dashed area is roughly 39% of the total number of electrons.

A one-dimensional statistics was tailored to describe a two-dimensional statistical problem resulting in a means to characterize the scattered electrons. To analyze the population of the scattered electrons, a one-dimensional standard deviation technique is employed in two orthogonal directions. The data is fitted to a linear regression curve that naturally passes through the mean position of the electron ensemble. An equation of a line perpendicular to the regression curve at the mean point is determined. All electron locations are projected onto the two orthogonal curves. The one-dimensional standard deviation is determined along the two lines separately yielding the lengths of the major and minor axes of an ellipse. A *dashed ellipse* is drawn on the scatter plots as show in Fig. 13. If the distribution is Gaussian, the ellipse (circle) will contain 39% of the electrons. Percent values are provided in Fig. 13. [Note for comparison: In a standard one dimensional problem characterized by a Gaussian distribution, 68.27% of the points will lie within the standard deviation of the distribution.]

Figure 13 presents typical SEE data from niobium at 360 $^\circ$K. It is argued that if secondary electrons exhibit truly random low energy trajectories, then one may be able to separate the backscattered electrons from the "true" secondary electrons by subtracting one from each bin with one or more collected electrons. If a bin contains more than one electron in a single shot with a time duration that is long enough to contain a statistical population of electrons but not too long to create

24

a situation that populates a large majority of the bins with more than one charge, then the bin count minus one yields the number of backscattered electrons (BSE). If a bin contains more than zero electrons, one electron in the bin is classified as a "True" secondary electron ("True" SE).   These conditions are depicted in Fig. 13.

The following conclusions were conjectured from the research effort for a measurable temperature range from 293 ^{o}K (room temperature) to ~360 ^{o}K:

- The "True" secondary electron distribution (as we define it) tends to exhibit a shifted Gaussian-like distribution for the surface grade under test;
- There are indications that a metal structure undergoing transient cooling exhibits some small overall average tendencies on the scattering process;
- Although not conclusive, the change in the mean number of scattered electrons seems to increase on average as the metal sample cools;
- The backscattered electron bunch appears to be scattered normal to the sample surface as depicted in Fig. 14.

Based on this study, the segregation of high energy backscattered electrons from the low energy "true" secondary electrons is geometrically possible assuming that the surface structure of the material is smooth. Such segregation allows one to focus on the type of coatings that are best suited for the physics of interest whether it be to enhance electron emission or inhibit electron emission.
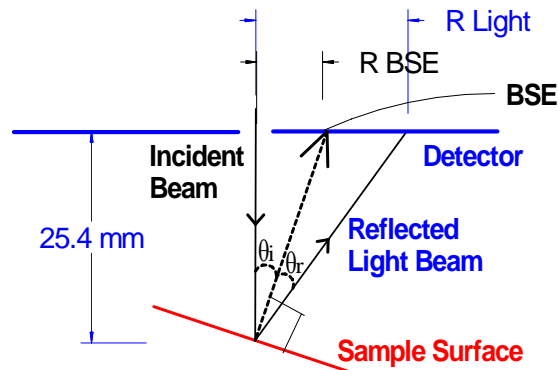

Fig. 14 Illustrating Snell's law of reflection for light relative to the backscattered secondary electrons based on experimental observations from smooth surfaces.

V. Collaboration with AFRL – Anode Coatings to Inhibit Secondary Electron Emission in High Power Microwave Devices

The AFRL's Materials and Manufacturing Directorate in Dayton Ohio (Dr. Steven Fairchild [AFRL], Dr. John Boeckl [AFRL], Dr. Timothy Peterson [AFRL], Dr. Kent Averett [AFRL], and Dr. Howard Smith [Triboligix Inc.]) and UNLV have teamed up to pursue thin film coatings and their inherent scattering properties so to minimize secondary electron emission or strategically redirect the emission in order to optimize the function of the anode in high power microwave tubes. AFRL developed small sample holders with varying grades 0°, 10°, and 30°. On each grade, four different coatings over an oxygen free Cu substrate were examined. Three of the four coatings (TiN, AlTiN, and TiCN) were deposited on thin, flat rectilinear copper slabs. The fourth sample was a Ti and Cu laminate-like structure (Ti and Cu multi-layer film) with a relatively small radius of curvature compared to the slabs. With the exception of the sample with curved surface, each sample was examined in the same manner. The sample holder is oriented with respect to a rectilinear coordinate system such that the grade of the sample is along the x axis. The curvature of the Ti-Cu laminate sample is also aligned with respect to the x axis and the grade of the holder. In all cases, no grade exists with respect to y. Holding y constant, x was varied. A labeling convention was

chosen to coordinate the sample test with target height relative to the detector. As the test number increases, the distance between the sample area targeted and the detector increases. A similar convention is chosen for the Ti-Cu target as well. Figure 15a displays the testing convention for the TiN, AlTiN, and TiCN samples whereas Figs. 15b and 15c display the testing convention for the Ti-Cu sample with curvature. The testing pattern in Fig. 15c is not necessarily the same for all grades supporting the Ti-Cu laminate sample. For comparison, studies were also conducted on a UNLV polished copper wedge with a 30° grade. As observed in Fig. 15d, the copper surface is not highly polished as indicated by visible grain marks in the surface. Further, the copper was not of oxygen free grade. Some of the mounted samples tested are displayed in Fig. 15. It is well known that rough surfaces typically inhibit secondary electron emission since there is a high probability that primary electrons and the secondary emission they produce in the valley of the grains will be captured by the neighboring grain walls in subsequent collisions. In effect, the grain valleys act similar to inverted Faraday cups. Smooth metal surfaces typically have high SEE yields. Although rough surfaces on bulk anode material are attractive for inhibiting SEE, high power microwave heating of the walls may degrade the desired surface roughness thereby influencing the behavior of the anode especially if the melting temperature of the material is low. The x and y coordinates provided in the figures are based on micrometer readings of the XYZ precision manipulator supporting the sample holder.
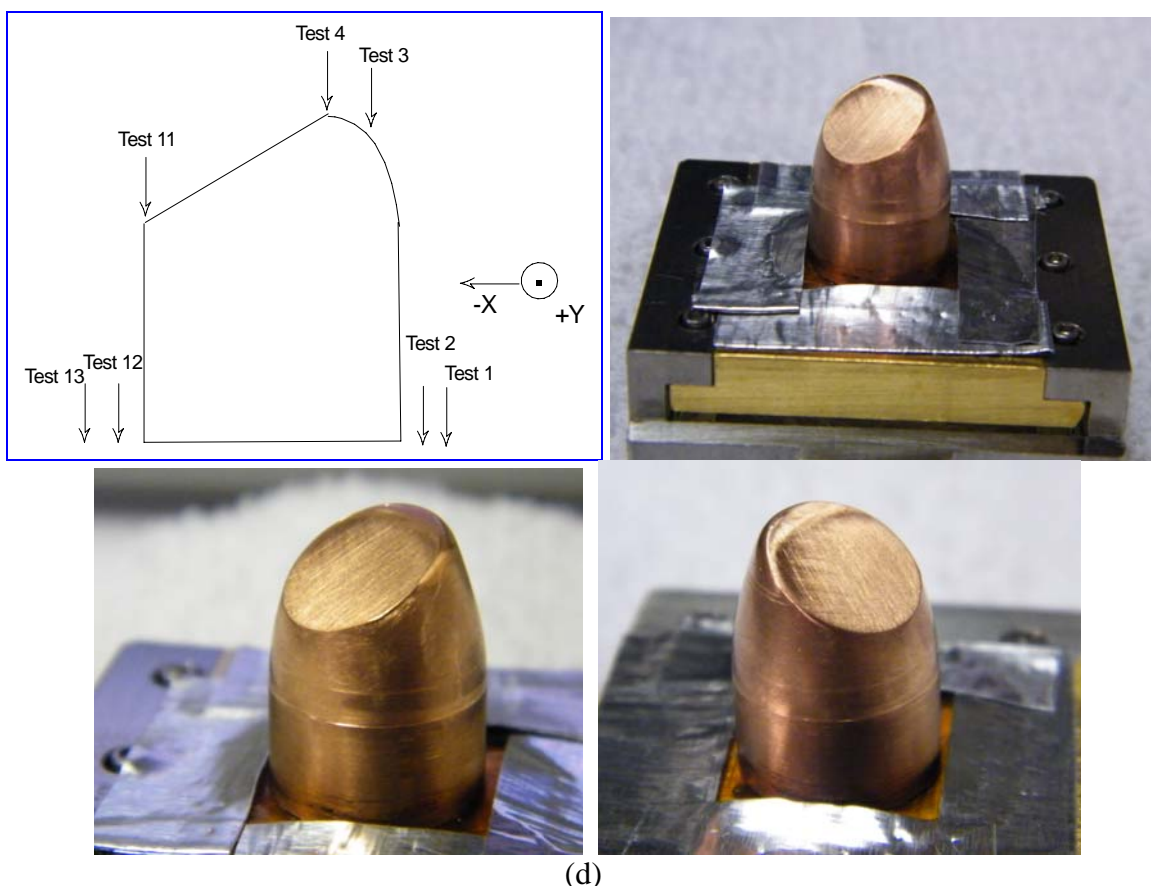

(a)

(b)

(c)

26

(d)
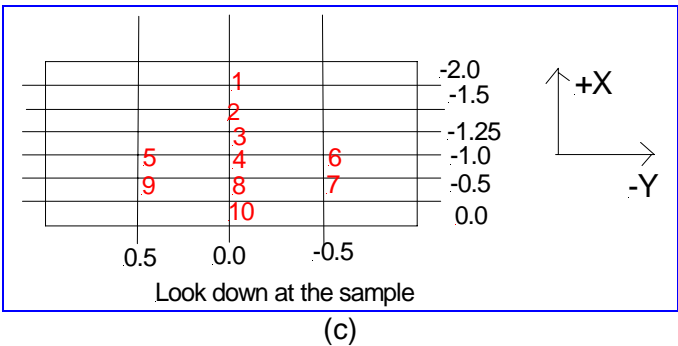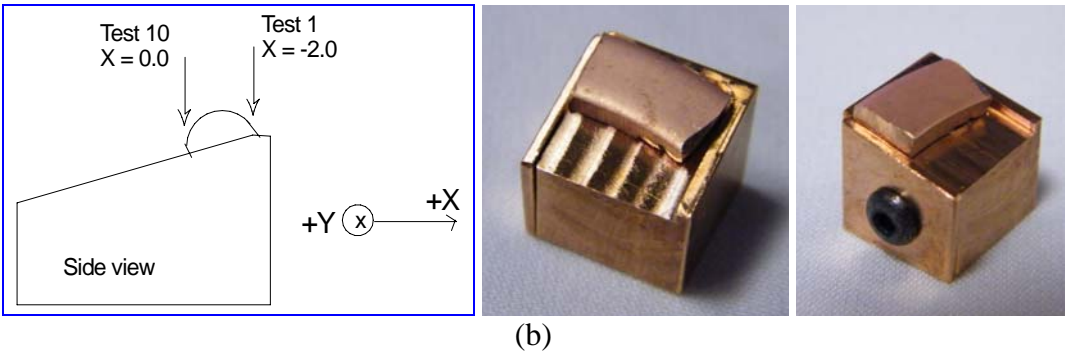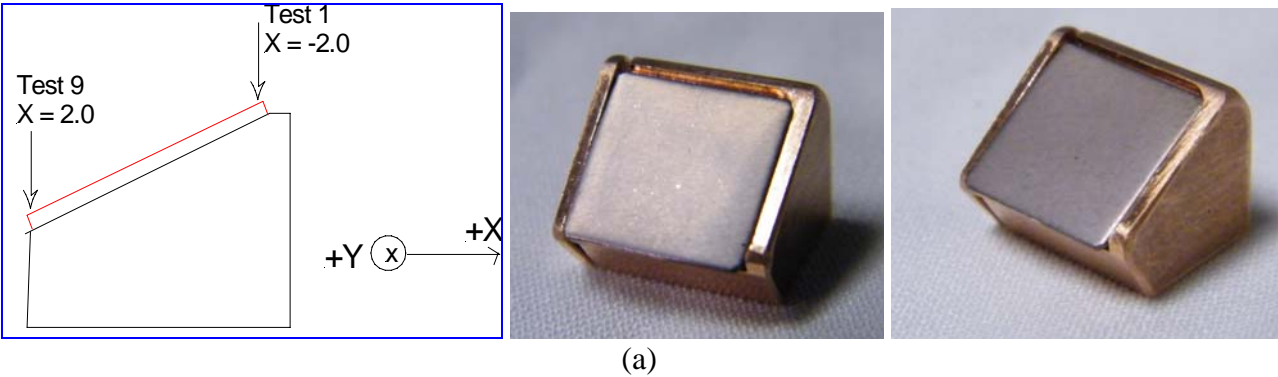
Fig. 15a-c Typical testing pattern convention for a) the side view for TiN, AlTiN, and TiCN samples, the b) side view, c) top view for the TiCu sample, and, for comparison, d) the UNLV polished solid copper wedge. Pictures of the samples and test stand are displayed. In each of these cases, the grade of the test stand is 30°. The copper wedge is not mounted on the AFRL test stand. Note the grainy nature of the copper wedge's surface. In the case for (a), the x location is varied and y is held constant typically near the central location of the sample. In all cases, Test 1 starts near the top of the grade which is the closest point to the particle position detector whereas Test 10 is at the furthest point from the particle position detector both in terms of distance in the z direction.

The many hundreds of tests performed over a six month plus period require some form of organization and consolidation in order to provide qualitative and quantitative measurements. Due to the care taken to maintain a very low current beam, relative and absolute measurements are provided. The four coatings were examined for low secondary electron emission count, uniform and nonuniform cluster formation of secondary electrons, repeatability of clustering, surface conditioning as a result of continuously illuminating the same position with a low current pulsed electron beam, and any apparent changes in the coating process over random positions on the sample. In all cases, multiple tests were performed on a sample mounted on a single test stand before breaking vacuum allowing for consistency in environmental conditions. Tests were performed at vacuum pressures below 3e-7 Torr. For single and multiple emission tests (single and multiple pulsed primary electron beam) at a single location, the primary electron beam energy, current, and pulse width are typically, 500 eV, constrained between 0.2 to 0.65 pA, and 100 ms respectively. [Refer to Appendix B regarding some specifics for the emission tests reported.] The electron beam has roughly a 150 μm diameter. The top of the sample holder is 2.5 cm from the detector grid. Specially shielded tri-axial cable connects the sample and grid to the electrometers allowing for monitoring the sample and grid currents. All ports including feedthroughs were required to be shielded with Al foil to minimize external penetration of noise into the chamber. Special grounding techniques were applied internal to the chamber to minimize and prevent Faraday induction effects that could result from a number of factors including acoustic vibration (microphonic effects). The grid voltage is either

0 V (grid off) or 150 V (grid on). The surfaces of the samples were carefully treated and mailed to UNLV. Thin films of TiN, AlTiN, TiCN and the Ti-Cu multilayer film were prepared on a highly polished, planar, oxygen free copper substrate (excluding the metal layer sample) at Wright-Patterson Air Force Research Laboratory and then mailed to UNLV in protective packaging. The materials remained in there protective packages until ready for experimentation. Human intervention resulted in hand-gloved transferring of the piece to a UHV vacuum chamber. Once mounted on the test stand with desired grade, all experimentation for that particular test stand is performed with the same vacuum environment. The used sample is stored either in a vacuum environment or in a desecrator with nitrogen environment until further testing.

Figures 16a-c and 16d-f provides typical series of three data sets, one for each grade, for the samples AlTiN and TiN. It is observed that the grade of the test stand influences the location of the center of gravity of the secondary electron emission as displayed by the mean position of the charge denoted with a red X on each of the graphs. The dashed elliptical (circular) geometry provides the demarcation of the one-dimensional standard deviation along the major and minor axis. For the AlTiN, the secondary electron emission count for the 30° grade is substantially larger than the other grades. This is due to the presence of the aperture in the detector. As observed in Fig. 16c, the center of gravity of the cluster of charge tends to shift off of the detector axis. In comparison, the TiN film appears to have the opposite characteristic. Care must be taken in interpreting the count and requires the simultaneous study of each grade. As indicated by Fig. 14, the backscattered electrons appear to be emitted on average normal to the surface at least for smooth surfaces. Therefore, Figs. 16a and b display the outer perimeter of the true secondaries with the anticipated primaries filtered from the data. [The primaries are directed into the detector hole.] On the other hand, the TiN film appears to disperse the effect of the primary electron beam in generate backscattered secondary electrons. (Refer to Figs. 16d-f.) The shift in the center of mass of the charge distribution as the grade increases yields fewer total secondary electrons which tend to be spread out over a larger area of the surface. Surface studies are being pursued at the Wright Patterson AFRL to determine if the TiN film has a grain-like characteristic that would result in electron dispersion or the ability for enhance energy deposition relative to other films. In comparison, Figs. 17a-b provide the electron scatter plots for the copper wedge with a nearly 0° grade and a nearly 30° grade surface. At nearly 30°, the concentration of the electron beam is tight and well within the standard deviation area (also to be defined as the 'significant emission area'). It is observed that the total secondary electron count of the copper wedge is typically larger especially for the 30° grade where the effect of the hole in the detector is less apparent for the thin film and wedge mediums. As indicated earlier, it is well known that rough surfaces tend to minimize secondary electron emission since electrons caught between material grains are captured within a few collision events with the grain wall. An energy study will allow for a more satisfying response since the true secondary electrons are typically low energy electrons well below 50 eV. Although not pursued during the period of this research endeavor, it is possible to reverse bias the controlling grid in the UNLV SEE Test Stand to a degree and study the energy distribution of the scattered electrons. With this interpretation in mind assuming that the surfaces are similar in shape, Figs. 18a-c suggests that TiN has nearly the lowest backscattered electrons (Fig. 18c) but has a relatively moderate secondary electron emission that is greater than AlTiN. Interestingly although AlTiN has a lower true secondary electron emission (Figs. 18a,b), its backscattered electrons is relatively significant (Fig. 18c). This effect is observed regardless of the voltage state of the grid. Keep in mind that the Ti-Cu sample can not be evaluated on the same level since its cylindrical surface does not conform to the uniform grade of the test stand.
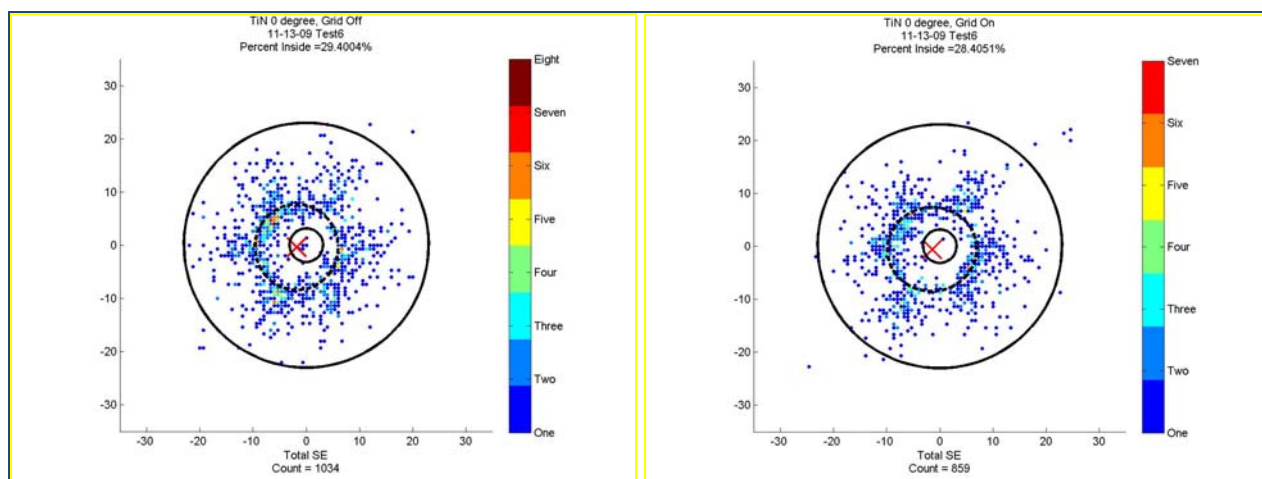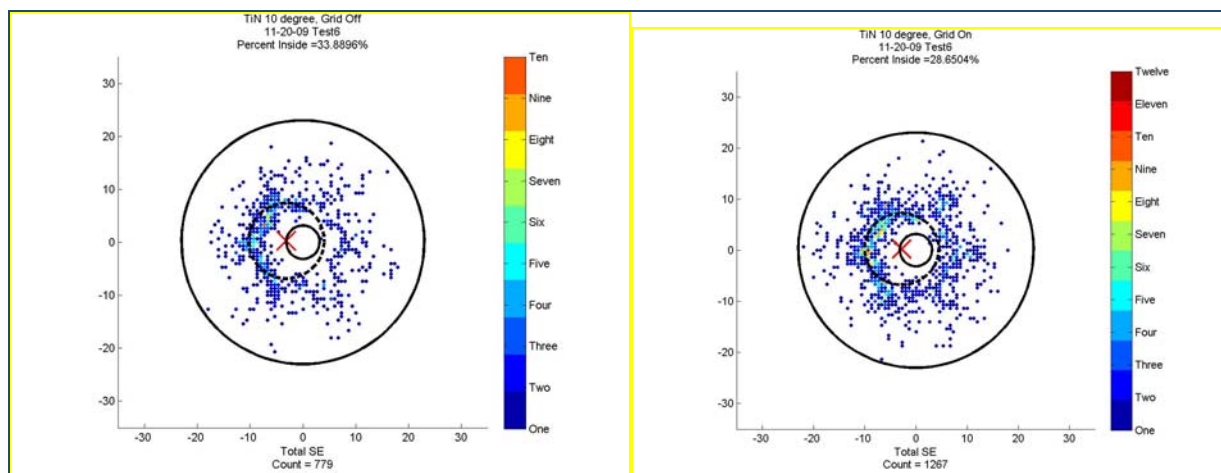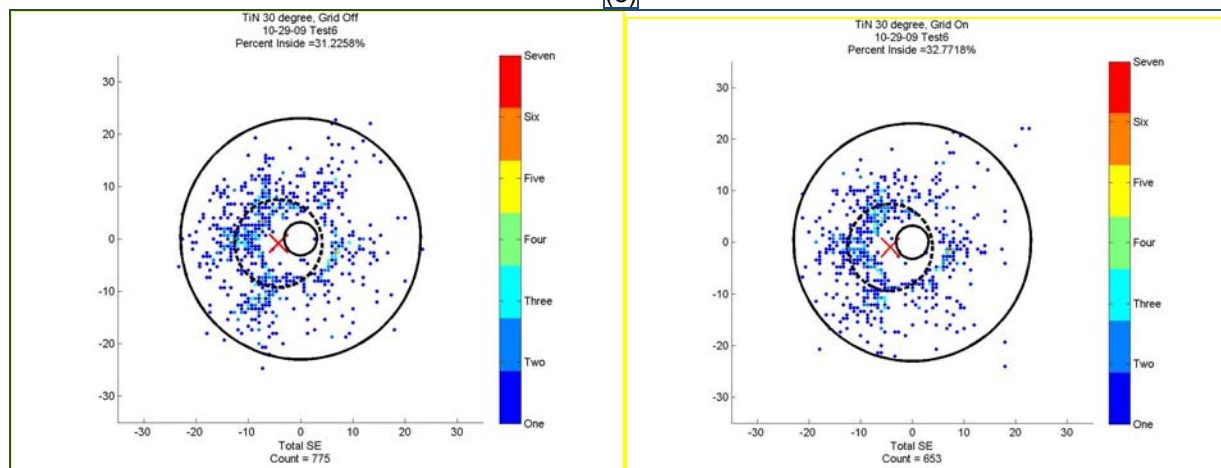
(a)

(b)

(c)

29
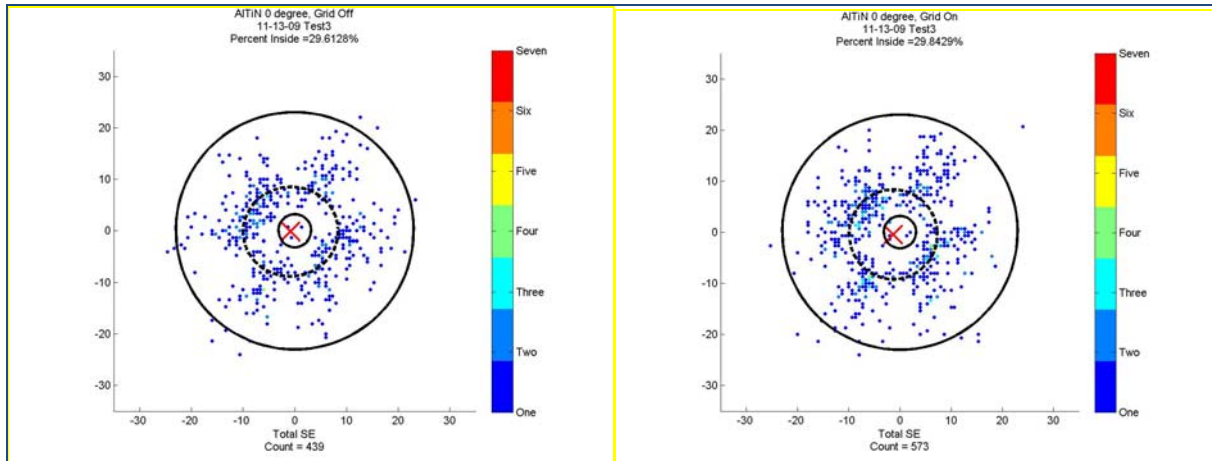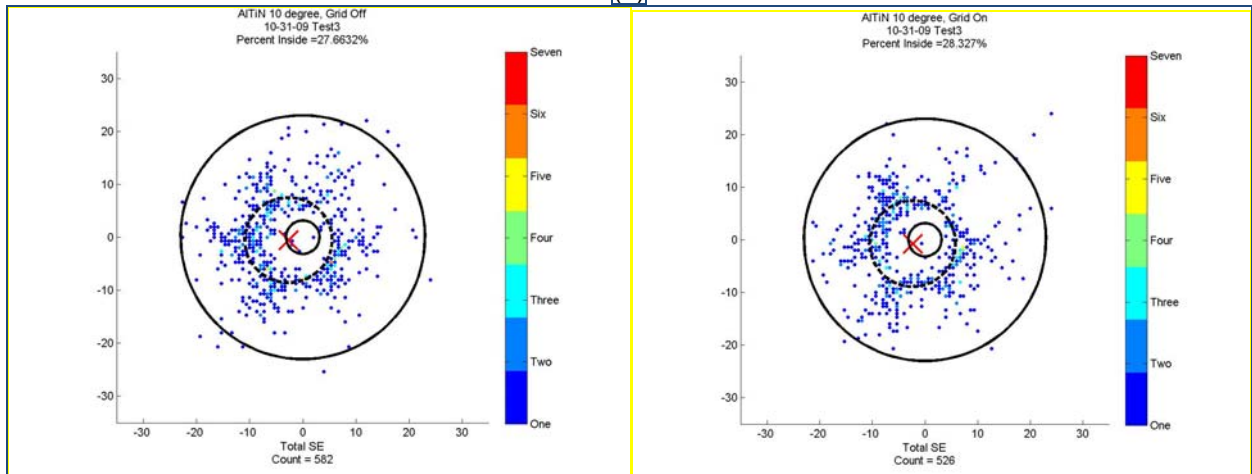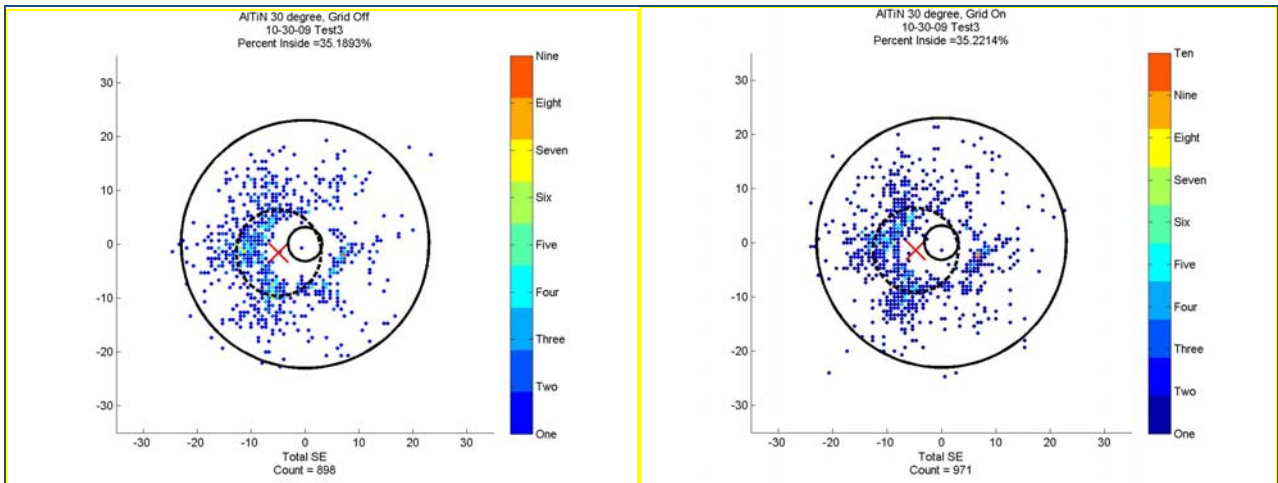
(d)

(e)

(f)

Fig. 16 a-f Provides a complete secondary electron emission study for AlTiN from each of the grades, a) 0° (439 count left; 573 count right), b) 10° (582 count left; 526 count right), and c) 30° (898 count left; 971 count right) at a single location. Similarly, a complete secondary electron emission study for TiN from each of the grades, d) 0° (1034 count left; 859 count right), e) 10° (779 count left; 1267 count right), and f) 30° (775 count left; 653 count right) at a single location are presented. In all cases, the condition when the grid is biased at 0 V (grid off) is on the left leaving the 150 V grid bias cases (grid on) on the right. The red X is the mean position (center of mass) of the detected secondary electron ensemble.
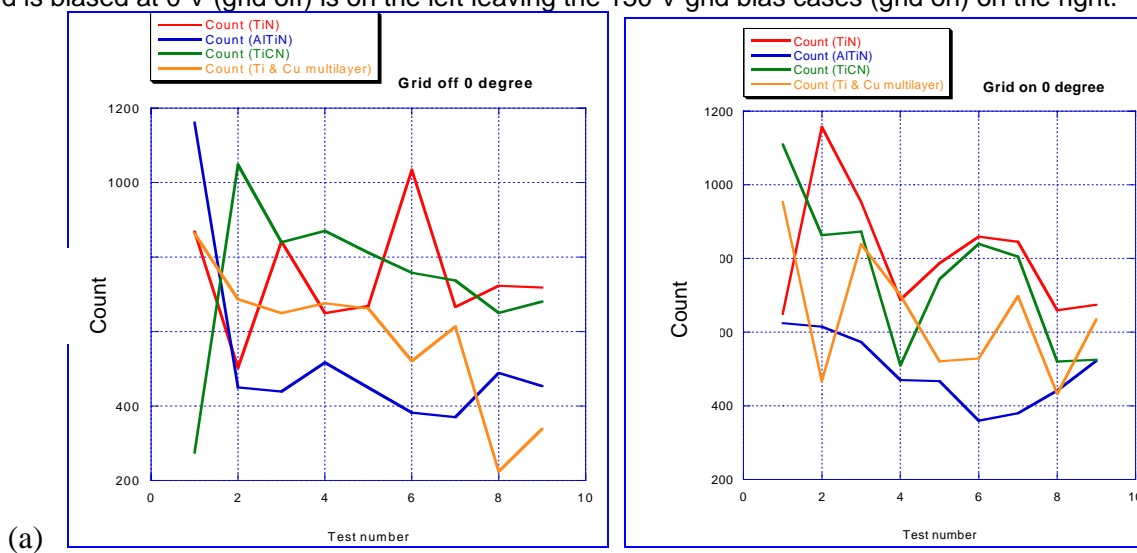
30
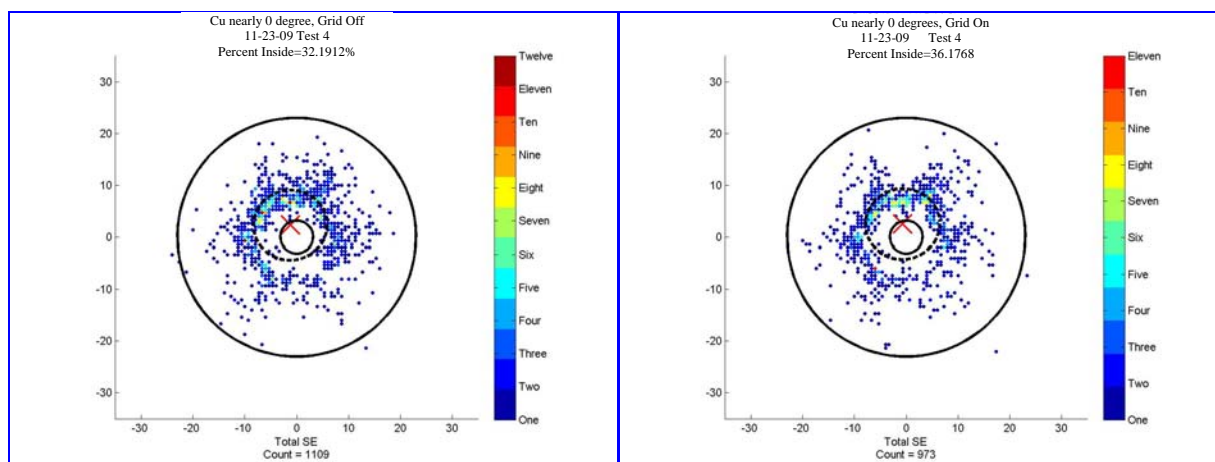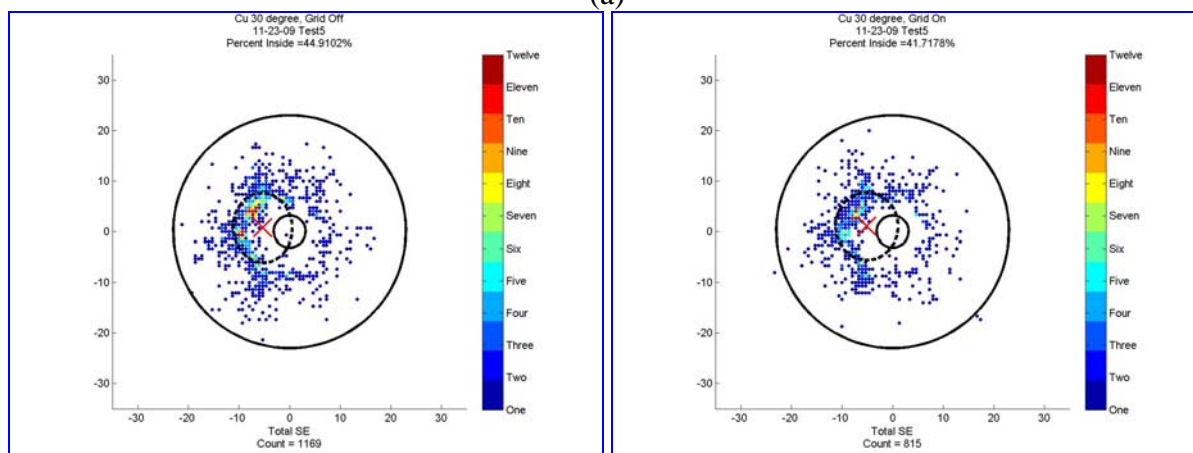
Fig. 17 a-b For comparison, a UNLV polished copper wedge was examined at a) nearly 0° grade (1109 count left; 973 count right) and b) nearly 30° grade (1169 count left; 815 count right). In all cases, the condition when the grid is biased at 0 V (grid off) is on the left leaving the 150 V grid bias cases (grid on) on the right.
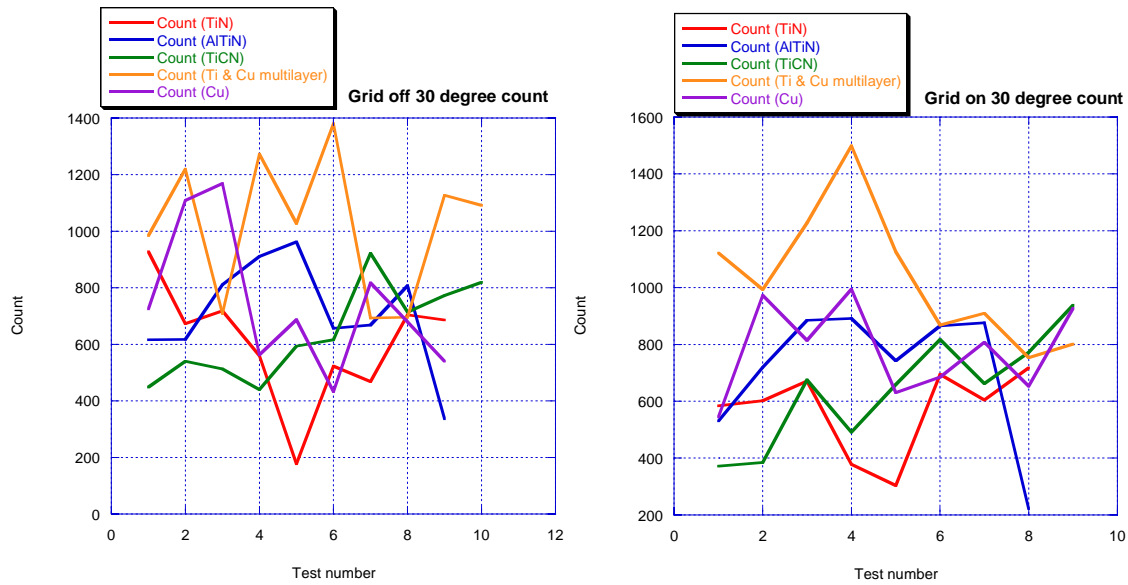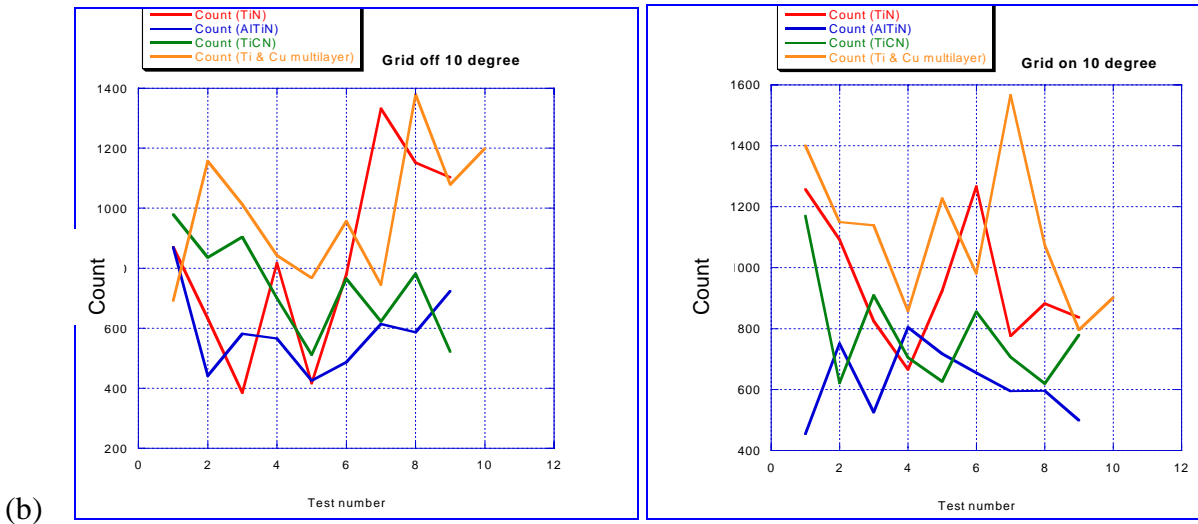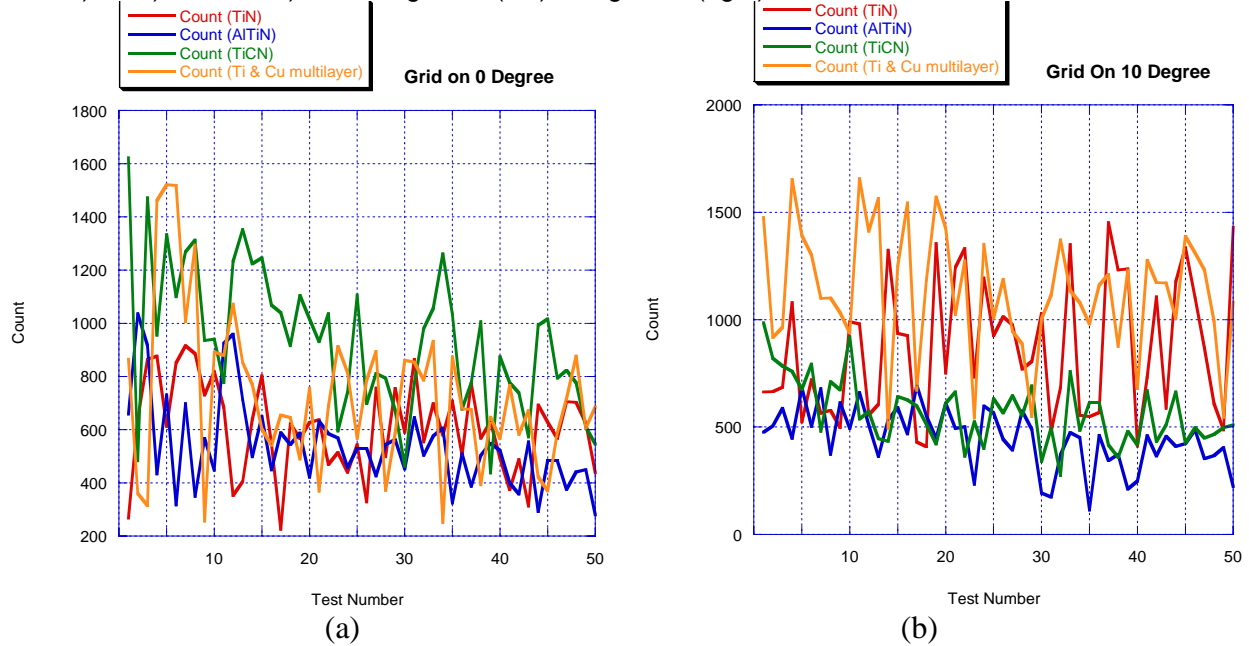

(a)

Fig. 18a-c A comparison of secondary electron emission count from a virgin emission point for sample holder grades a) 0°, b) 10°, and c) 30° with grid off (left) and grid on (right).

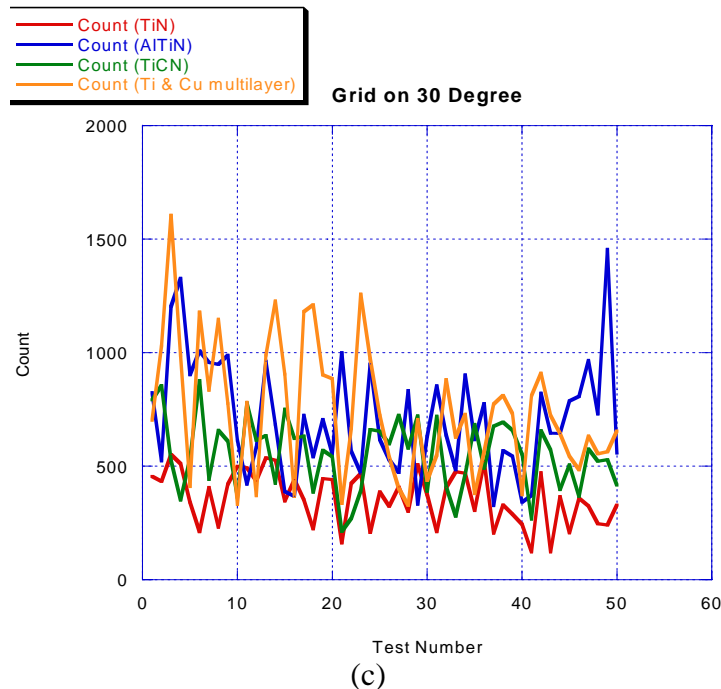(a)

(b)

Grid on 30 Degree

Fig. 19a-c Fifty, 0.3 to 0.5 pA, 100 ms electron beam pulses were directed at a single location to study the change in the electron emission over time due to multiple electron beam stimuli for the a) 0°, b) 10°, and c) 30° grades.

Although crude, Figs. 19a-c examines the SEE characteristics as the sample is bombarded with fifty low current, low energy pulses of primary electrons. For each of the grades, a single location was chosen at random to be probed. It is observed over the duration of the fifty pulses that TiCN, Ti on Cu multilayer, and to a lesser degree AlTiN exhibit a decrease in average secondary electron emission count with increase in primary beam illumination. TiN does not necessarily offer the same characteristic as observed in Fig. 19b. It is observed that the average TiN SEE count increases with pulse illumination for the 10° grade as compared to the other two grades. Based on Fig. 16e and the initial emissions of Fig. 19b for TiN (10° grade), the secondary electron emission appears to be enhanced on average and very unstable. More multiple emission tests at 10° are warranted to determine if this is a material characteristic with angle dependence or if the coating is flawed or non-uniform at that particular position.

Figure 20 focuses on TiN and AlTiN when multiple emission tests are performed at a single location and when single emission tests are performed at multiple locations. Each grade is shown on the same plot for comparison. Secondary electron emission appears to be angle dependent for TiN and, at least for the one multiple emission test case, secondary emission from TiN is undesirably enhanced relative to other grades (Fig. 20a). As far as single emission tests are concerned (Fig. 20b), the 30° grade appears to be on average lower in count than the other two grades. In comparison, AlTiN appears to have significant angle dependence as far as single emission tests are concerned but, as multiple emission tests tend to show, the material tends to harden after multiple emission tests. Assuming one can extrapolate, the material looses its grade dependence. TiCN has a similar multiple emission characteristic as AlTiN. Note, the color coding between the 0° and 10° degrees in the multiple and single emission plots are different.
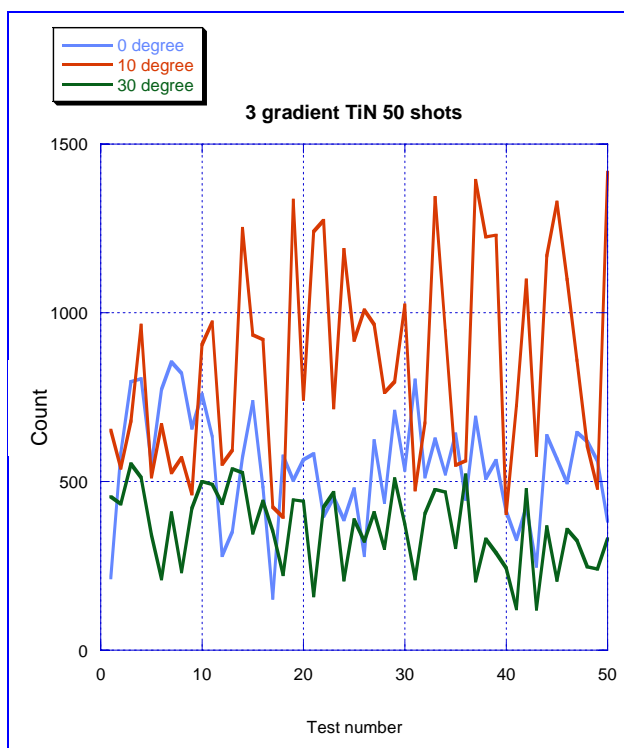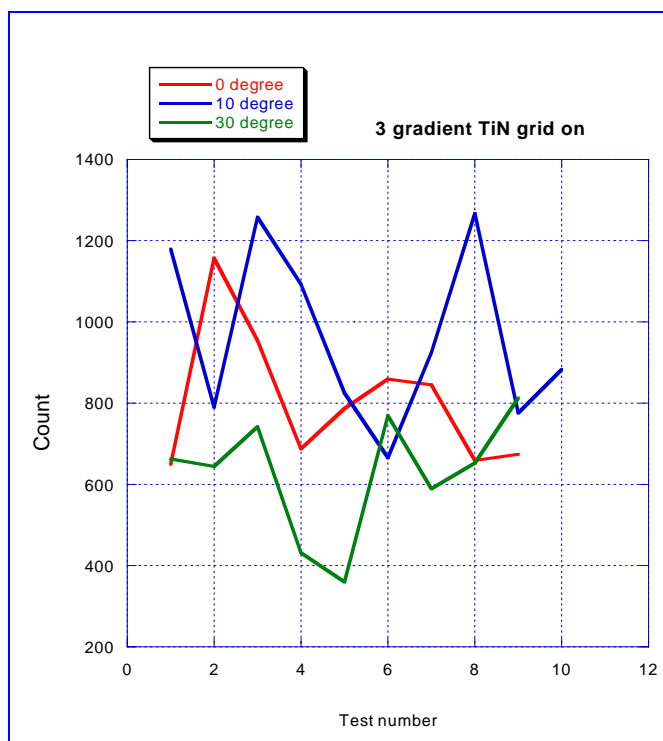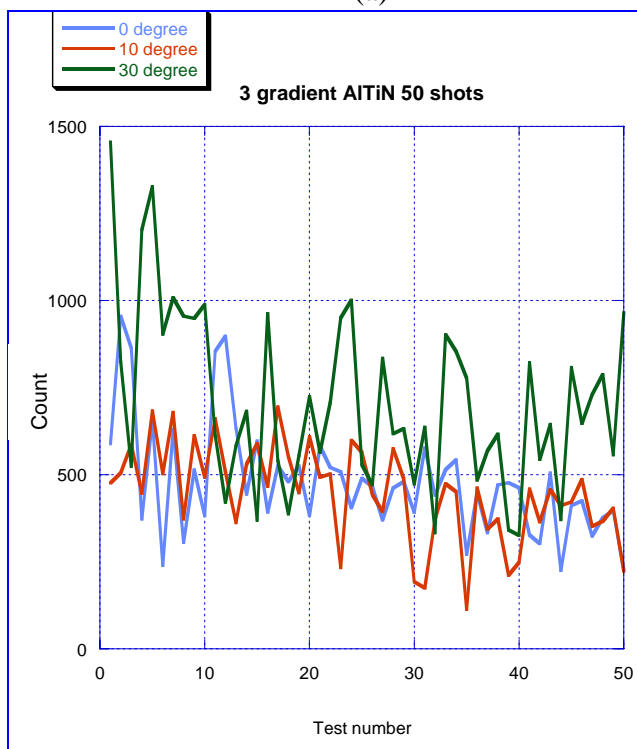
Fig. 20a-d Single and multiple emission tests are considered for TiN (a and b) and AlTiN (c and d). Both materials have different characteristics that tend to change as multiple, low current, low energy, emission tests are performed. The grid is biased at 150 V in all cases. Note, the legends of the single and multiple emission test are different.
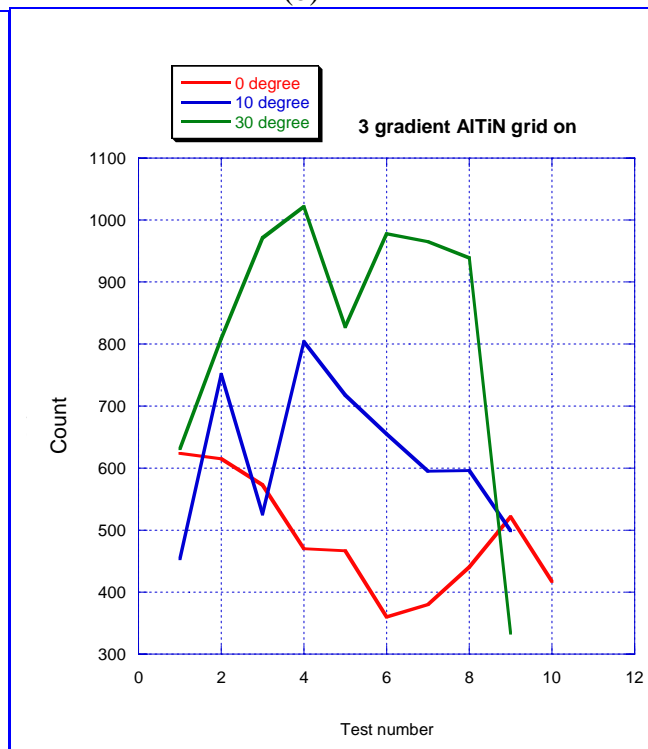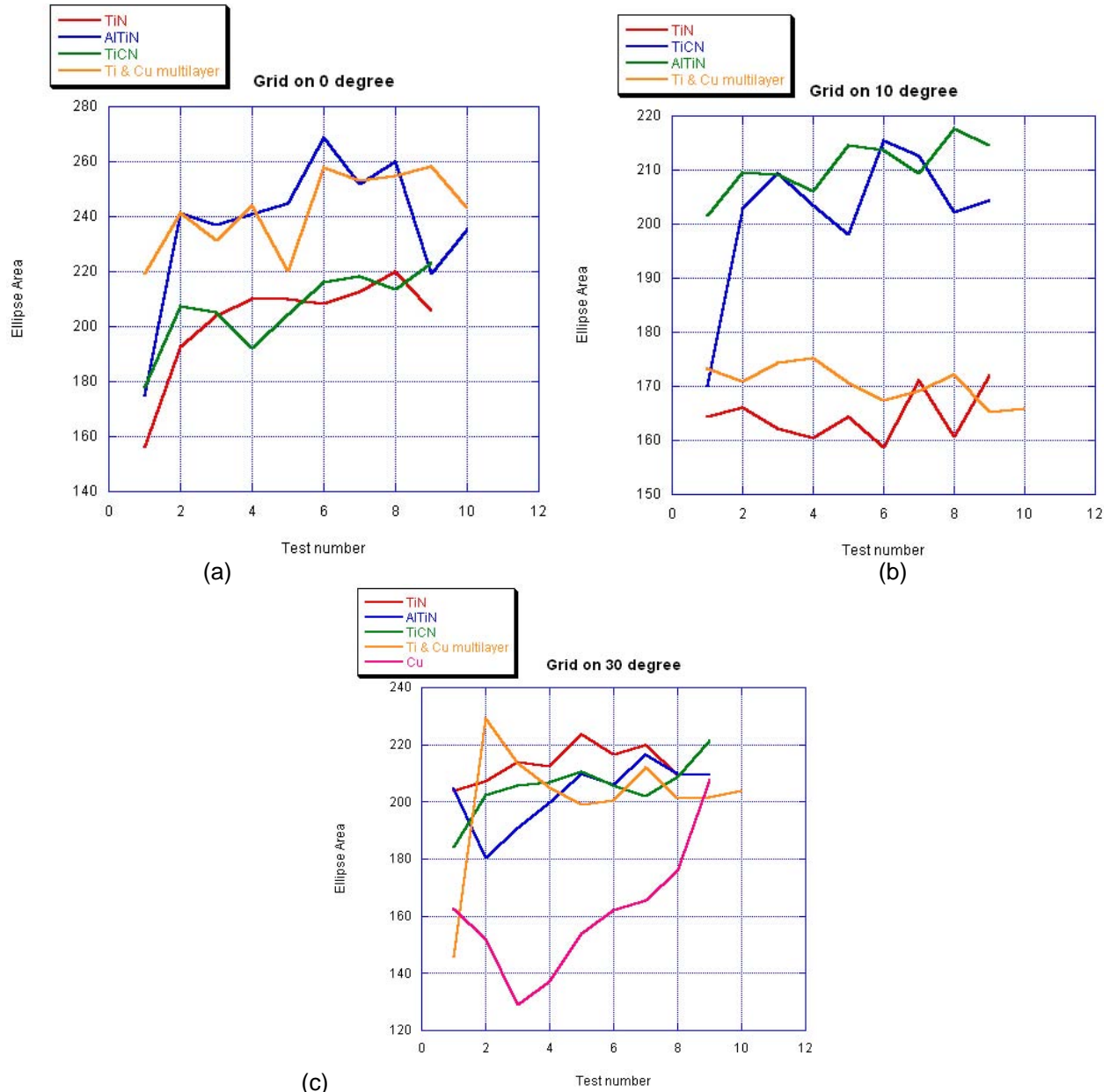
Fig. 21a-c The physical planar area where 39% of the charge reside if the charge distribution is a two-dimensional Gaussian distribution. The length of the major and minor axis is determined by the projections of the points onto a linear regression line and a perpendicular line. The intersection between the two lines is the mean position of the detected secondary electron charge ensemble.

Although count is an important measurable, it does not provide a complete picture regarding secondary electron emission. The compactness of the electron cluster, cluster drift, and mean position of the cluster offers information regarding certain aspects of surface morphology, surface physics, surface uniformity and degradation. The elliptical area based on two one-dimensional standard deviations povides a measure regarding the compactness of the emitted secondary electron cluster about its mean position as identified by a red X in Figs. 16 and 17. In principle, the smaller the standard deviation is about the mean, the smaller the area, and hence the more compact the secondary electron distribution is about the mean. This assumes that the elliptical area is somewhat circular. For simplicity, we will label the elliptical area (standard deviation area) as the 'significant emission area'. It is observed in Figs. 16 and 17 that the circumference of each emission test is somewhat circular.   In all cases, it is observed that the elliptically bounded region bounds all or a part of the hole in the detector. This implies that if the distribution is indeed Gaussian, a

35

significant number of electrons are not detected due to the presence of the hole in the detector. As anticipated, as the grade of the test stand is extended to 30°, the closely clustered secondary electrons, presumeably the backscattered electrons, begin to significantly populate the detector surface. As observed in Figs. 21a-b for the 0° and 10° grades, the 'significant emission area' of TiN is significantly smaller than that for AlTiN and TiCN thin films. Because of the non-planar geometry for the Ti- Cu laminate, the interpretation of the measure is not appropriate. It was pointed out that the emission of true secondary electrons are statistical in nature and the back scattered electrons have a more predictable scattering pattern. Therefore, it is suggested that the backscattered electrons are lost through the hole. It is possible that the thin film absorbes the backscatted electrons but this is unlikely. Clearly, in Fig. 21c, the copper wedge (without a thin film) has a highly focused backscatted electron cluster. Consequently, by comparison, this implies that the thin films tend to significantly affect the collision cascade of the primary electron as it passes into the sample under test. A temperature study of the anode when illuminated with and without the coating would offer some insights to the amount of energy absorbed by the different samples. Since the 'significant emission area' is larger, it would seem reasonable to hypothesize that either the thin film surfaces are microscopically rough offering the primary beam many different surfaces to be emitted from or that a significant amount of energy has been deposited into the thin film to directing the primary electrons in a much wider plethora of scattering directions. By examining the samples in Fig. 15a-c, the copper sample has a visibly significant grain pattern than the other samples. The AFRL is examining the samples' surface for roughness and patterns.

(a)   (b)
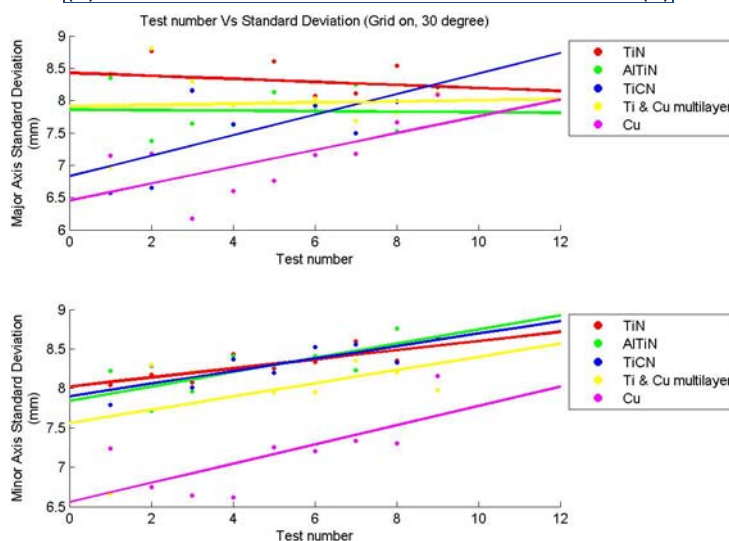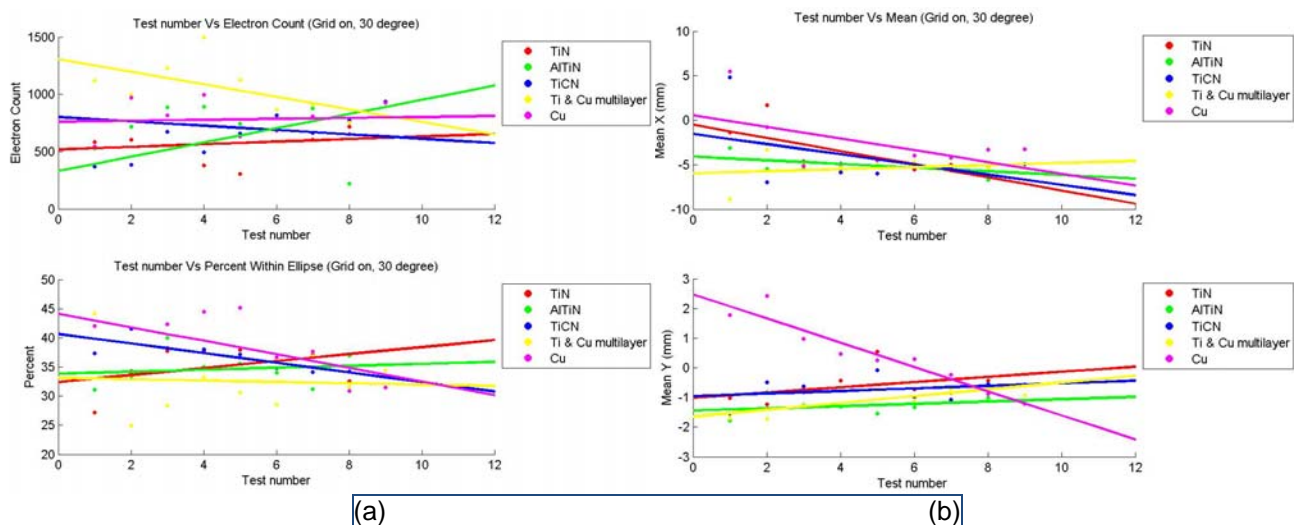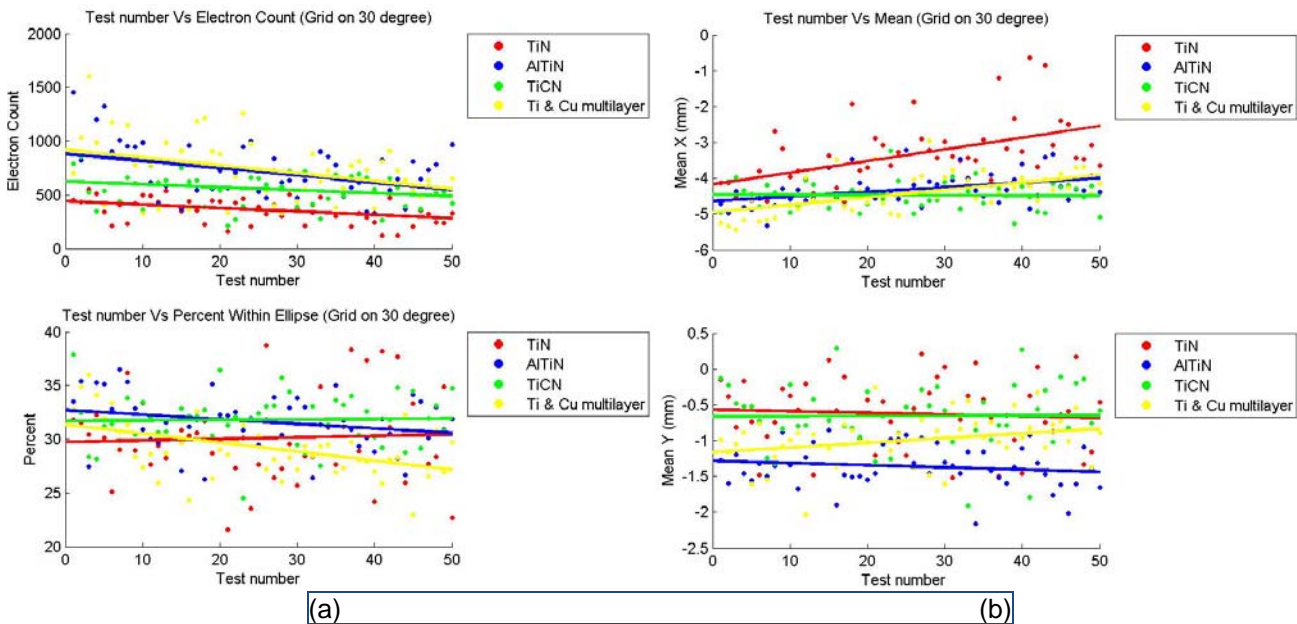

(c)

Fig. 22a-c A comparison study of the statistics regarding the distribution of the SEE cluster for single secondary electron emission tests from a number of different locations with the sample mounted on the 30° grade test stand. Results are reported with a biased grid (grid on).

Figure 22a-c provides a statistical study based on eight to ten randomly located, single emission tests from samples mounted on a 30° grade sample holder with a 150 V grid bias. [As a reminder, Ti-Cu laminate was included only for casual comparison.] Based on this study, the secondary electrons from TiCN appear to be closely clustered with minimum drift of the cluster's mean position. This tends to indicate that the surface medium is uniform and possibly not grainy to the primary electron. Even so, the standard deviation along the major and minor axes is not constant and tends to rise on average as the test number increases.

For a 30° grade, AlTiN has nearly the highest secondary electron emission count over all emission tests (refer to Fig. 23a top) at a single location. But, these counts are more contained then that for other films (refer to Fig. 23a bottom and Fig. 23c). The location of the mean position of the secondary electrons (refer to Fig. 23b) appears relatively stationary with the y position but tends to vary a little in x with a low standard deviation along both the major and minor axes of the 'significant emission area'. Relative to the other coatings, this seems to imply that although the electron count for this grade is high, the scattered cluster appears to be more directed than the other films with a reasonable standard of deviation. The film tends to direct the secondary population with less dispersion. Based on the premise that a "true" secondary electron is emitted in a random direction with low emission energy, the class of electrons being well directed are backscattered electrons. An energy analysis is warranted to determine if the electrons composing the relatively confined secondary electron cluster are backscattered electrons. Multiple emission tests on the copper wedge were not performed.

(a)   (b)
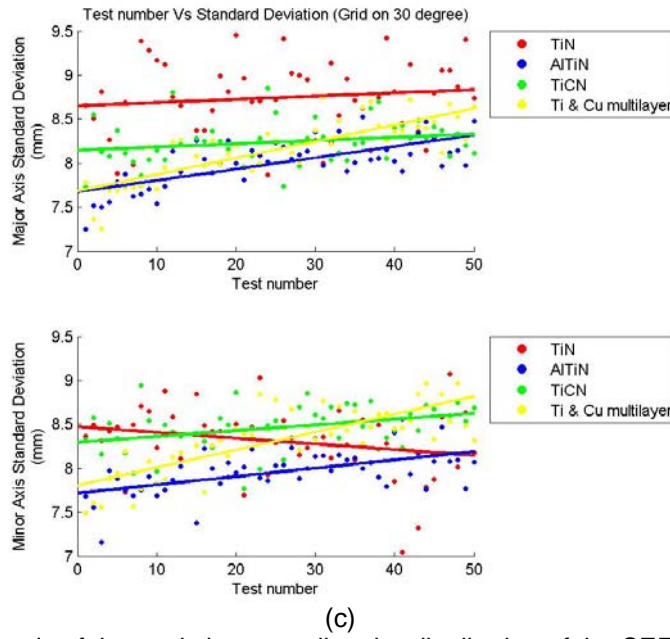
(c)

Fig. 23a-c A comparison study of the statistics regarding the distribution of the SEE cluster for multiple electron emission tests from a single random location with the sample mounted on the 30° grade test stand.

V. Conclusion

With the research studies concluded, we now summarize the effort by addressing in part the primary questions asked motivating the effort.

1. *How do primary sources of pulsed electrons alter the surface and/or bulk properties of a material under test over time and affect energy deposition mechanisms of the medium? Can one implement these properties to condition or recondition the surface of the sample minimizing undesired emission processes?*

2. *What influence do contaminants, coatings and composites, and thermal gradients have on SEE?*

Based on the secondary electron emission studies in this effort, added information regarding the distribution of the secondary electron emission may be used as a tool in examining the surface physics of materials, in particular, metals and good conductors. Secondary electron emission may be inhibited or enhanced as certain thin films are conditioned with multiple low current, low energy electron illumination. Secondary electron emission appears to depend on the primary electron beam's angle of incidence with the macroscopically smooth coated surface. In all cases especially for smooth surfaces, backscattered electrons on average tend to be scattered in a direction normal to a planar metal surface at least for primary beam energies on the order of 0.5 to 1 keV and temperatures between 360 °K and room temperature. This may be used as a means to segregate the low energy "true" secondary electrons from the backscattered secondary electrons offering alternative means to manage the different energy loads of the scattered ensemble better. The "True" secondary electron distribution (as we define it) tends to exhibit a shifted Gaussian-like distribution for the surface grade under test. There are indications that warm metal structures undergoing transient cooling exhibit some small overall average tendencies on the scattering process. Although not conclusive, the change in the mean number of scattered electrons seems to increase on average as the metal sample cools. Comparing the AFRL coated films against a UNLV polished, grainy, copper wedge, the thin films tend to minimize the SEE count relative to the copper wedge with a less focused secondary electron cluster. In high power microwave devices, the

38

current density may be high enough smooth over rough copper surfaces. Not only can thin films and composites mechanically and thermally extend the longevity of the anode, it can also manage the beam load. Even so, not all films have the same characteristics based on pulsed, 100 ms, subpicoampere primary electron beams. Surface studies of the samples tested at UNLV are underway at the AFRL. It is hypothesized that the nature of the surface grains of the different films may influence the overall properties of the scattering process especially if different molecular structures or sub-layers are favored near the interface for the different coatings examined. This influence is also a function of the uniformity of the film, the film thicknesses, and the orientation of the crystalline surface of the film in the path of the electron beam.

References:

1. <u>High-Power Microwave Sources and Technologies</u>, ed. Robert J. Barker and Edl Schamiloglu, IEEE Press, New York, 2001, Chapts. 1-4, 10 and 12.
2. S.D. Korovin, V.V. Rostov, S.D. Polevin, I.V. Pegel, E.Schamiloglu, M.I. Fuks and R.J. Barker, "Pulsed Power-Driven High-Power Microwave Sources," *Proc.of the IEEE*, 92, 7, July 2004, 1082.
3. Rudberg, E., "Characteristic Energy Losses of Electrons Scattered from Incandescent Solids," *Proceedings of the Royal Society of London. Series A, Containing Papers of a Mathematical and Physical Character*, vol. 127, issue 804, pp. 111-140, Apr. 1930.
4. Rudberg, E., "Inelastic Scattering of Electrons from Solids," *Physical Review*, vol.50, pp. 138-150, Jul. 1936.
5. Zerda, T.W. *Stefan Boltzmann Law*, Texas Christian University, 2001 http://personal.tcu.edu/~zerda/manual/lab22.htm
6. J. W. Davis and S. Fabritsiev, <u>Pure Tungsten - Electrical Resistivity. ITER Material Properties Handbook</u>. University of California, San Diego. http://fusionnet.seas.ucla.edu/fusionnetwork/iter_materials.php?code=ST-M-RF-%23201-0108P-0100
   [References provided therein:
   i. V. A. Sorkin, "Tungsten Technical Data (in Russian)," Technical Report of VNIITS, Moscow , 1988.
   ii. Properties of Elements (in Russian), Ed. G. V.Samsonov, Moscow , Metallurgy, 1976.]
7. H. Padamsee, J. Knobloch, and T. Hays, <u>RF Superconductivity for Accelerators</u>, John Wiley, New York, 1998, p. 183. [Original source: <u>CRC Handbook of Chemistry and Physics</u>, 65th ed.]

APPENDIX A

POSTER SLIDES FOR ICOPS 2009
[International Conference of Plasma Science, San Diego, CA, May 31 – June 5, 2009]

Slide 1

ELECTRON STIMULATED SECONDARY ELECTRON EMISSION FROM A WARM METAL SURFACE*

Shaoru Garner, Robert A. Schill, Jr., Sean Andersen, Kris Buchanan, and Jackie Schill

University of Nevada Las Vegas
Department of Electrical and Computer Engineering
4505 Maryland Parkway
Las Vegas, NV 89154-4026, USA
schill@ee.unlv.edu

Slide 2

Introduction and Hypothesis

- Heat removal in metal structures is often the limiting factor in high power, high frequency microwave tube devices. Larger output powers may be realized for brief periods in time at the expense of operating in a pulsed power and/or pulsed cooling mode. During these brief periods, temporary temperature fluctuations on the walls of the microwave tube are realized.

- *It is hypothesized that the temperature fluctuations and to a much lesser extent temperature gradients may influence secondary electron emission resulting from primary electrons colliding with the microwave wall.*

- Supporting statement: Low energy primary electrons, that penetrate the microwave wall, experience the collective effects of the electrons (plasmons) in the conduction band of the metal. It is anticipated that the surface temperature of the metal wall influences the ability for plasmons to interact with the primary electron in the scattering process.

Garner, Schill, Andersen, & Buchanan   ICOPS 2009 SEE from Warm Metal Surface   2

Slide 3

Experimental Setup

A 0.1s pulsed 500 eV, 0.4 to 0.63 pA primary electron beam is directed towards the niobium sample under test with a 15° and 30° angle of incidence relative to the surface normal. Low beam currents are used to examine collectively the change in the spatial distribution profiles of secondary electrons as the sample cools without significantly modifying or stressing the sample surface. A flat copper plate with a sharp contact edge acts as a thermal source to the sample decreasing the thermal time constant of the experiment.   A pulsed 1 kW, 9 GHz, 6% duty cycle (100 kHz PRF, 600 ns PW) microwave source drives a TE_{10} mode in a shorted waveguide with 4cmx2.3cm broadwall aperture that covers and heats a portion of the thermal copper storage plate surface with sample extending into the waveguide. Peak temperatures well over 400° K are attained but due to long detector biasing procedures measurable peak sample temperatures cool to about 360° K. With appropriate thermal insulation, a cryostat supporting the sample and sample holder is used as the cooling reservoir to control the thermal properties of the sample. With the aid of a 0V or 150 V extraction grid, SEE distributions are measured during transient cooling.

Garner, Schill, Andersen, & Buchanan   ICOPS 2009 SEE from Warm Metal Surface   3

Slide 4

Artist's 3D Rendition of the UNLV SEE Test Stand

4

Slide 5

UNLV SEE Test Stand

Waveguide for Sample Heating

Electron Gun & Beam Drift Tube

Particle Position Detector Assembly

Sample

Manipulator & Cleaning Arm

Thermal Storage Plate

Sample Holder

Cryostat
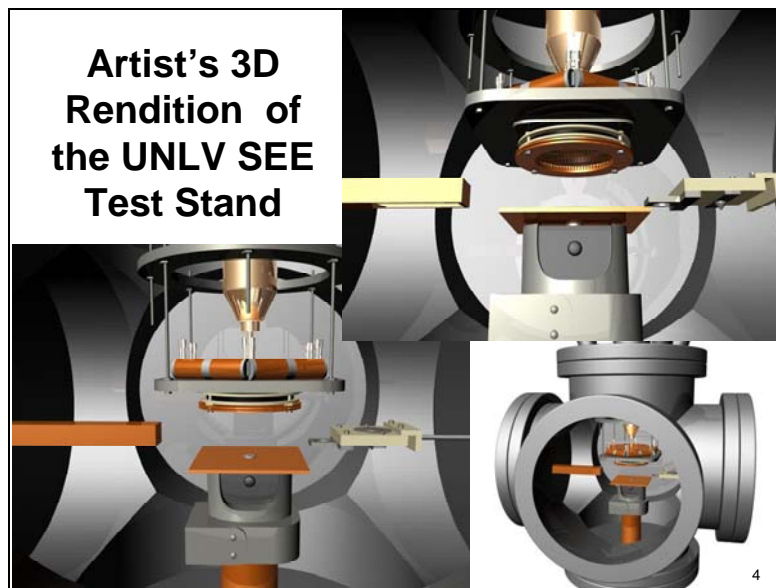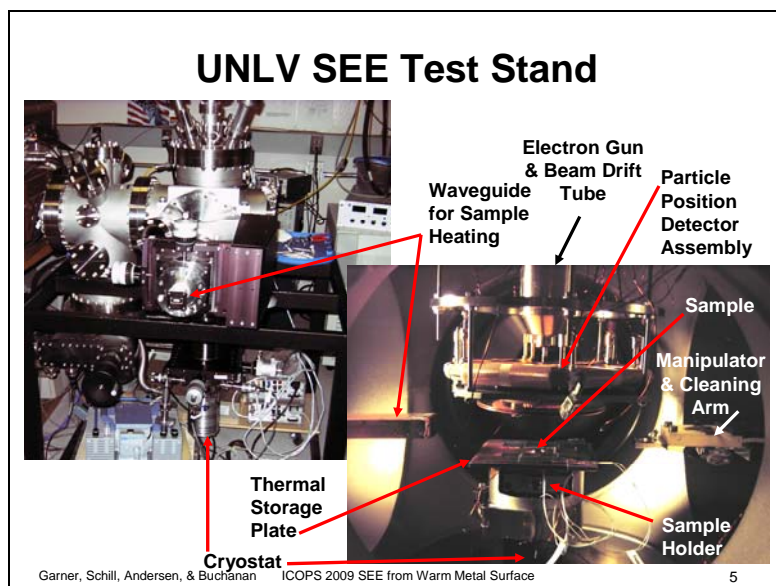
Slide 6

Preparation of Niobium Sample Surface

0.5 mm reticle

The buffered chemical polished sample as viewed through a long distance microscope. The sample supports a 0°, 15°, 30°, and 45° surface grade.

- 2005 Buffered Chemical Polish Niobium Sample (LANL)
  - Surface removal - 98 microns
  - 1:1:2 ratio hydrofluoric acid, nitric acid, phosphoric acid
  - Temp. 8 - 10° C
- Intermittent period 2005 – 2009
  - Exposed to atmosphere
  - No special treatment
- Preparation for Experiment 2009
  - Clean surface with 200 proof alcohol
  - Outgas sample in at pressures below 5×10^{-7} Torr environment for about one hour or longer
  - Purge surface with Ni for about 5 minutes after each set of runs with chamber pressure not exceeding 2×10^{-6} Torr.

Slide 7

Analyzing 2D Scatter Data

- To analyze the population of the scattered electrons, a one dimensional standard deviation technique is employed in two orthogonal directions. The data is fitted to a linear regression curve that passes through the mean position. An equation of a line perpendicular to the regression curve at the mean point is determined. All points are projected onto the two orthogonal curves. The one dimensional standard deviation is determined along the two lines yielding the lengths of the major and minor axes of an ellipse. A *dashed ellipse* is drawn on the scatter plot. If the distribution is Gaussian, the ellipse (circle) will contain 39% of the electrons. Percent values are provided in the following figures. [Note for comparison: In a standard one dimensional problem characterized by a Gaussian distribution, 68.27% of the points will lie within the standard deviation of the distribution.]

Slide 8

Classification/Identification of Sec. Electr. (1)

- As the primary electron enters the impinging medium, inelastic scattering processes ensue based on a collision cross-section probability. Next generation secondary electrons are generated. Elastic scattering processes also exist resulting in the change of direction of the primary electron and a loss of kinetic energy. All existing generations of secondary electrons undergo such a scattering process as well. Although weakened, the identity of the primary electron in the scattering process is maintained due to its improbability to impart most of its energy in any one single collision process. If emitted from the surface of the sample, this electron is denoted as a backscattered electron. Based on the retention of the primary electron's identity even though the scattering events are large and the scattering processes are random, one expects a high probability that all similar primary electrons should experience a similar collision cascade process resulting in a similar scattering process. Consequently, backscattered electrons should exhibit a particular spatial distribution pattern. Further, all following generations of secondary electrons are randomized with a high probability of being imparted relatively small energies. If these secondary electrons are emitted from the sample, they usually have low energies and are denoted as true secondary electrons. Due to the random motion of the secondary electron in the sample, a random emission pattern should exist.

Slide 9

Classification/Identification of Sec. Electr. (2)

- A 0.1s, 0.5 pA rectangular electron beam contains about 312,500 electrons. Assuming uniform gun emission, an electron is generated every 320 ns. The distance between the sample and the detector is about 2.54 cm. In this 320 ns time duration, a 1 eV electron can travel the round trip distance about 3.7 times. The time duration between first contact and emission is negligible and the scattering yields are assumed low (less than 5). Therefore, at these low currents, one can imagine that the emitted secondary electrons may be treated as isolated single particles; space charge effects do not exist.

- Based on the single particle nature of the problem and the anticipated scattering pattern that may result in the scattering process, we distinguish the true secondary electrons from the backscattered electrons as follows:

  If a bin contains more than one electron in a single shot, then most of the electrons in the bin are identified as backscattered electrons (BSE). The number of backscattered electrons in the bin is the number of electrons detected in the bin minus one.

  If a bin contains more than zero electrons, one electron in the bin is classified as a "True" secondary electron ("True" SE).

Slide 10

15° Grade, Grid 0V_{5/28/09}

X - center-of-mass location
% - Percent counts in ellipse

608   37.8%   207   41.1%   401   33%

Seven
Six
Five
Four
Three
Two
One

Room Temp. 290° K (TOP) [SE Count: 608, 207, 401]

Total SE   *BSE*   *"True" SE*
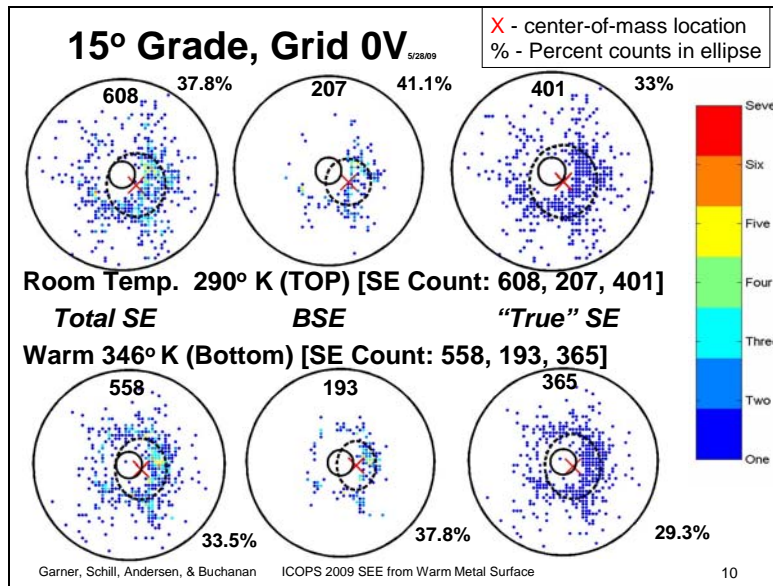
Warm 346° K (Bottom) [SE Count: 558, 193, 365]

558   193   365

33.5%   37.8%   29.3%

Garner, Schill, Andersen, & Buchanan   ICOPS 2009 SEE from Warm Metal Surface   10

Slide 11

30° Grade, Grid 0V_{5/29/09}

X - center-of-mass location
% - Percent counts in ellipse

672   40.9%   256   41.4%   416   37.5%

Seven
Six
Five
Four
Three
Two
One

Room Temp. 290° K (TOP) [SE Counts: 672, 256, 416]

Total SE   *BSE*   *"True" SE*

Warm 360° K (Bottom) [SE Counts: 546, 218, 328]

546   218   328

43%   34.4%   38.4%

Garner, Schill, Andersen, & Buchanan   ICOPS 2009 SEE from Warm Metal Surface   11

Slide 12

BSE Location- Smooth Surface Approx.

- Snell's Law
  - Light reflected from a mirror
  - 30° grade (beveled) surface
    - Location R_{Light}=44 mm, clearly off detector surface
- Location of BSE
  - Central location of BSE bunch appears to be located more normal to the sample surface.
  - 30° beveled surface
    - For Beam on detector axis, R_{BSE}=15 mm, is just beyond the region of the BSE cluster

R_{BSE}=15mm

Axis units - mm

Backscattered SE

R Light
R BSE
BSE
Incident Beam
Detector
25.4 mm
Reflected Light Beam
θ_i θ_r
Sample Surface

$$R_{Light} = 25.4 \tan(2\theta_i)\,[mm]$$

$$R_{BSE} = 25.4 \tan(\theta_i)\,[mm]$$

$$\theta_i = \text{degree grade}$$

Garner, Schill, Andersen, & Buchanan   ICOPS 2009 SEE from Warm Metal Surface   12

Slide 13

**Transient Cooling Study Total SE –
Averaged over Three Data Sets 15° Grade**

- Grid voltage = 0 V ; A data set is defined by a unique dot color.
- Primary beam impacted the sample at the same position for each data set
- Room temperature test was conducted last

Garner, Schill, Andersen, & Buchanan   ICOPS 2009 SEE from Warm Metal Surface   13

Slide 14

**Transient Cooling Study BSE – Averaged
over Three Data Sets 15° Grade**

- Grid voltage = 0 V ; A data set is defined by a unique dot color.
- Primary beam impacted the sample at the same position for each data set
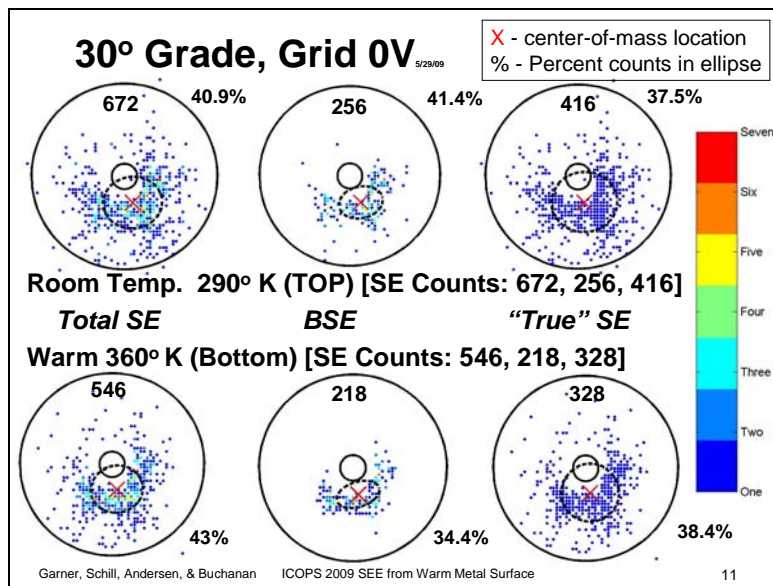- Room temperature test was conducted last

Garner, Schill, Andersen, & Buchanan   ICOPS 2009 SEE from Warm Metal Surface   14

Slide 15

**Transient Cooling Study "True" SE –
Averaged over Three Data Sets 15° Grade**

- Grid voltage = 0 V; A data set is defined by a unique dot color.
- Primary beam impacted the sample at the same position for each data set
- Room temperature test was conducted last

Garner, Schill, Andersen, & Buchanan   ICOPS 2009 SEE from Warm Metal Surface   15

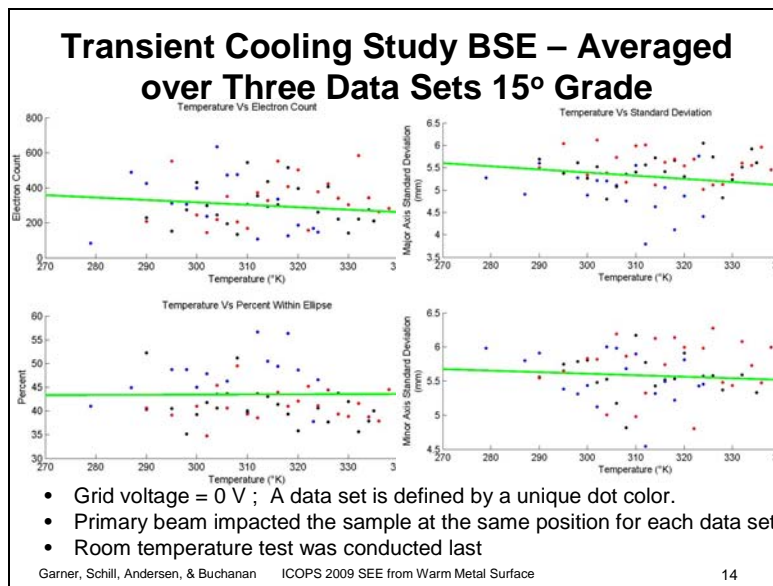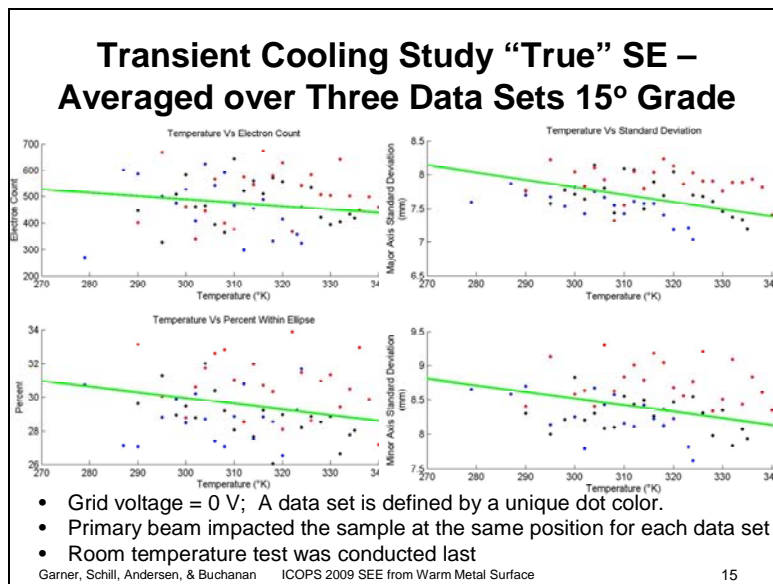Slide 16

15° & 30° Grade Overall Observations
**Independent of SE Classification**

- Mean count varies slightly (typically increases) with decrease in temperature (from 360° and 290° K) (0% to 15%)
- The elliptical area containing the concentration of secondary electrons increases with decrease in temperature
- The mean location of the center of mass tends to shift with temperature. Average location of mean at each temperature tends to be at a different location for each data set
- Tendencies are similar regardless if the grid extraction voltage is zero or 150 V.
- It appears that the "True" SE distribution from the 30° grade tends to yield a more Gaussian like behavior. Note that the center of mass of the average electron with elliptical (near circular) distribution concentration contains a small fraction of the central hole in the detector as compared to the 15° grade.

Garner, Schill, Andersen, & Buchanan   ICOPS 2009 SEE from Warm Metal Surface   16

Slide 17

Assumptions &
Exp. Errors

- The position of the sample along the beam axis is initially adjusted for each data set. This adjustment results in a positioning error which in turn causes movement of the SE distribution's center of mass. A linear regression curve is fitted to each data set for comparison. Note that the change of position with temperature is similar for each data set.
- Uniformity of primary beam current assumed.
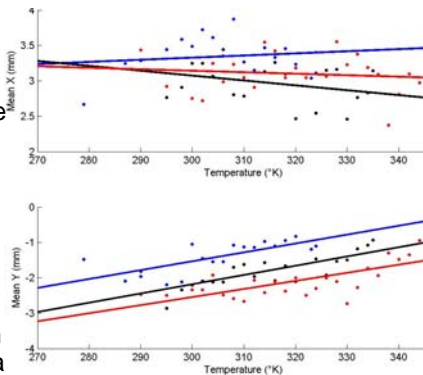
- Approx. sample surface smooth
- Assumed, primary beam currents do not alter sample surface.
- Thermal expansion/ contraction effects are negligible for T from 290° to 400° K.

Garner, Schill, Andersen, & Buchanan   ICOPS 2009 SEE from Warm Metal Surface   17

Slide 18

Conclusions

- Influenced by the distribution of BSE based on how we define "True" SE, the "True" SE distribution tends to exhibit a shifted Gaussian like distribution for the 30° grade.
- There are indications that a metal structures undergoing transient cooling over a small range of temperatures (360° to 290° K) exhibits some small overall average tendencies on the scattering process.
- The change in the mean number of scattered electrons seems to increase on average as the metal sample cools. This is not conclusive in all experimental data sets.
- Backscattered electron bunch appears to be scattered normal to the sample surface

Garner, Schill, Andersen, & Buchanan   ICOPS 2009 SEE from Warm Metal Surface   18

46

APPENDIX B

AFRL EMISSION TEST DATA
UNLV Test Stand State Data and AFRL Sample Type
10/29/09 – 11/23/09

All shots are taken with beam pulse of 100ms.
Detector voltage (V): 300, 2200, 2200, 2500
Detector current (mA): 0.320, 0.012, 0, 0.001
Grid voltage (V) = 150
Room Temperature (K): 296
E = 500eV, If = 1.40A

| Date | Material | Sample holder Grade (deg.) | Shots location | | Vacuum Pressure (Torr) | Beam current (pA) |
			One Emission Test at each location	Fifty Shots at single location		
10-29-09	TiN	30	X	X	1.1e-7	-0.3556 ~-0.5973
10-30-09	AlTiN	30	X	X	5.5e-8	-0.4201 ~ -0.6195
10-31-09	AlTiN	10	X	X	9.8e-8	-0.3958 ~ -0.5644
11-02-09	TiCN	10	X	X	6.9e-8	-0.3169 ~ -0.5293
11-03-09	TiCN	30	X	X	8.0e-8	-0.3354 ~ -0.5938
11-05-09	TiCu	30	X		2.0e-7	-0.3387 ~ -0.6095
11-06-09	TiCu	30		X	4.5e-8	-0.2938 ~ -0.5336
11-07-09	TiCu	0	X		4.4e-8	-0.2984 ~ -0.5799
11-12-09	TiCN	0	X		1.4e-7	-0.3110 ~ -0.5783
11-12-09	Cu	0	X		4.6e-8	-0.3069 ~ -0.5143
11-13-09	AlTiN	0	X		4.7e-8	-0.2983 ~ -0.5418
11-13-09	TiN	0	X		1.4e-7	-0.3395 ~ -0.5287
11-16-09	TiN	0		X	3.8e-8	-0.3065 ~ -0.5378
11-17-09	AlTiN	0		X	5.8e-8	-0.3335 ~ -0.5987
11-17-09	TiCN	0		X	6.6e-8	-0.2987 ~ -0.5349
11-18-09	TiCu	0		X	2.6e-7	-0.2983 ~ -0.5436
11-20-09	TiCu	10	X	X	5.8e-8	-0.3559 ~ -0.5788
11-20-09	TiN	10	X		2.7e-7	-0.2983 ~ -0.5364
11-23-09	Cu/Wedge	30	X		2.3e-7	-0.3017 ~ -0.6019
11-23-09	TiN	10		X	5.9e-8	-0.3110 ~ -0.5483